Energy Conversion and Management 209 (2020) 112646

Contents lists available at ScienceDirect

Energy Conversion and Management

journal homepage: www.elsevier.com/locate/enconman

A dual-intake-port technology as a design option for a Sliding Vane Rotary Expander of small-scale ORC-based power units

Fabio Fatigati*, Marco Di Bartolomeo, Davide Di Battista, Roberto Cipollone

University of L'Aquila, Department of Industrial and Information Engineering and Economics, Via Giovanni Gronchi, 18, L'Aquila, Italy

ARTICLE INFO

Keywords:
Sliding Vane Rotary Expander Design
Downsizing
Dual Intake Port
Organic Rankine Cycle
Exhaust Gases Waste Heat Recovery
Friction Power Loss Reduction

ABSTRACT

Volumetric machines are the most suitable candidates to be used as expander in power units based on the Organic Rankine Cycle (ORC) thermodynamic concept, for waste heat recovery of Internal Combustion Engine in the on-the-road transportation sector. In particular, the technology of the Sliding Rotary Vane Expander (SRVE) shows intrinsic advantages thanks to their lower cost, shaping features, easier manufacturing and reliability and, generally speaking, very suitable operative conditions. Nevertheless, they show some disadvantages which are typical of volumetric machines, such as low capacity, limited expansion ratio and power lost by friction.

Among the different technologies available to reduce the effects of these aspects (revolution speed increase, elliptical stators or with more complex geometries, tip blade optimization, rolling stators, etc.), the Dual-Intake Port (DIP) was assessed as a promising solution to enhance SVREs performance and operability. However, dual-intake port was still not conceived as design option.

In this paper, a novel Sliding Vane Rotary Expander design concept involving a Dual Intake Port expander (DIP) option was developed and compared to the conventional Single Intake Port (SIP) one, under the same operating conditions. Thus, after an experimental comparison between SIP and DIP expanders, under the same conditions of mass flowrate, a theoretical expander model of the latter was validated on a set of experimental results. The model allows to outline the advantages of considering the dual port as a design option: for a specific flow rate and revolution speed, this option allows to reduce the friction losses, which represent a weak point of this volumetric machine. For a given mass flow rate of the working fluid, an additional feature is that it allows a sensible downsizing with respect to the SIP, with an axial dimension reduction up to 50%, ensuring additional weight and space saving. Despite the reduction of the dimensions, DIP produces a comparable mechanical power with respect to SIP, limiting the reduction to 8–10% of the SIP one with a 50% lower mechanical power loss due to friction. For the same flow rate, the added intake port determines a decrease of the intake pressure which is completely beneficial in terms of operating conditions of the overall recovery unit.

1. Introduction

Waste heat recovery (WHR) from the exhaust gases of Internal Combustion Engine (ICE) through ORC-based power unit is one of the most promising solutions to increase fuel energy savings and reduce CO_2 emissions [1]. In [2] an experimental study showed a 0.65% thermal efficiency increase in a 285 kW Diesel Engine with a WHR system based on an ORC power unit using R245fa as working fluid. Meanwhile a decrease of Brake Specific Fuel Consumption up to 3.6 g/kWh was experienced. Even though the net recovery efficiency is limited to few percentage points [3–5], the benefits is still interesting mainly for heavy duty engines and some steady or quasi-steady applications.

Nevertheless, unlike for large applications where ORC technology is quite conventional, there are still some difficulties which delay a visible development in the transportation sector. As reported in [6], these are related to the final use of the energy recovered on board (mechanical or electrical), the engine back-pressure produced by the evaporator on the exhaust gases duct, the encumbrance limitations, the increase of the vehicle weight and the significant variations of the high and cold thermal sources (exhaust gases and environment). In particular, these last issues lead to a transient behavior of the recovery unit which causes a decrease of the expected performance [7], partly recovered through the use of control strategies [8]. Transient behaviors depend mainly on the Heat Recovery Vapor Generator (HRVG), in which heat is exchanged from gases to working fluid producing its vaporization and

* Corresponding author.
E-mail address: fabio.fatigati@univaq.it (F. Fatigati).

https://doi.org/10.1016/j.enconman.2020.112646
Received 29 November 2019; Received in revised form 10 February 2020; Accepted 22 February 2020
Available online 06 March 2020
0196-8904/

Nomenclature

Symbols

A	Area [m^2]
C	Friction coefficient
D	Equivalent diameter [mm]
d	Diameter [mm]
dp	Pressure difference [MPa], [bar]
ecc	Eccentricity [mm]
F	Force [N]
h	Specific Enthalpy [kJ/kg]
k	Mass flow rate fraction
L	Length [mm]
m	Mass [kg]
$\dot{m}$	Mass flow rate [kg/s]
N_v	Vane Number
p	Pressure [MPa], [bar]
r	Radius [mm]
R	Specific gas constant [kJ/kgK]
t	Time [s]
T	Temperature [K]
Tk	Thickness [mm]
V	Vane volume [m^3]
V	Vane
W	Width [mm]
Z	Compressibility factor
tip	Contact region between blade and stator
vol	volumetric
WF	Working Fluid

Greek symbol

α	permeability
Δp	Pressure difference [MPa], [bar]
Δθ	Angular extent [deg]
η	Efficiency
θ	Rotational angle deg
μ	Dynamic viscosity [Pa·s]
ρ	Density [kg/m^3]
$\Phi_{dual\ int}$	Dual intake port position [deg]
ϕ	Dual intake control valve opening degree
ω	Revolution speed [rpm], [rad/s]

Subscript

1	Mass flow rate fraction entering main intake port
2	Mass flow rate fraction entering dual intake port
b	Blade
c	Centrifugal Force
dual int	Dual intake port
end	Port closing
ext,env	External enviornment
exh	Exhaust port
exp	Expander
g	Global
i	Generic i-vane
in	intake pressure or temperature
int	Intake port
ind	Indicated
is	Isentropic condition
loss	Loss
n	Normal
main	Main intake port
mech	Mechanical
out	Outlet
p	Pressure Force
rot	Rotor
start	Port opening
stator	Stator
v	Vane

Acronyms

AEG	Asynchronous Electric Generator
AEM	Asynchronous Electric Motor
ECU	Electronic Control Unit
DIP	Dual Intake Port Expander
DDIP	Downsized Dual Intake Port Expander
DSIP	Downsized Dual Intake Port Expander
HRVG	Heat recovery vapor generator
ICE	Internal Combustion Engine
ORC	Organic Rankine Cycle
SIP	Single Intake Port Expander
SVRE	Sliding Vane Rotary Expander
WHR	Waste Heat Recovery

superheating. According to a specific design of the recovery unit, it is easy to find operating conditions which don't guarantee the sufficient heat to vaporize (and superheat) the working fluid to the design conditions. The need to manage transient behaviors on the main thermodynamic properties due to the intrinsic delay produced by thermal systems is an additional issue. The expander technology (which firstly receive the working fluid from the HRVG), however, can partially overcome these off-design situations [9].

The expanders are generally classified in dynamic (axial and radial turbine) and volumetric machines, such as vane, scroll, screw and reciprocating piston expanders [10]. Despite dynamic machines represent the most used expander devices in steady-operated heavy-duty power plants, for a small-medium scale application, volumetric devices are generally preferred thanks to their lower revolution speed and higher capability to deal with off design conditions [11]. The simple geometry they have, with respect to the dynamic machines, implies a reduced cost which is a not negligible additional feature, mainly when the power of the unit is low (< 10–20 kW). On the other hand, main drawbacks of volumetric expanders are represented by the limited in-out volume ratio (expansion capability), swept volume, [12], vane filling (volumetric efficiency), [13], and lubrication needs [14] to keep friction losses under control (mechanical efficiency). In order to overcome these problems, many design and technological solutions were proposed and reported in literature. In [15] a step-by-step scroll design was presented and volumetric and mechanical losses - which can be minimized adopting a specific chamber height - were discussed. A novel symmetric discharge structure was proposed for scroll expander in [16] and numerically compared with a conventional unilateral discharge system. The results showed that this option allows to reduce operating pressure and secondary flows. It also ensures a drive torque enhancement up to 6.5%, which plays a positive role in efficiency performance. Concerning screw expanders, the throttling loss at the inlet port has been discussed in [17] showing the need for an optimization of the vane geometry. Rotor profiles [18] are among the most important factors to enhance machine volumetric and mechanical efficiency: in fact, a symmetric profile of a screw compressor led to significant leakages when the machine was adapted to behave as expander [19]. In order to reduce the leakages, an "N" profile was developed ([20,21]). In [22] a novel operational strategy of a twin-screw expander was presented: it consisted in the injection of pre-heated liquid into the machine (at

intermediate pressure level) in order to reduce the exhaust temperature, preventing thermal damages in the case a hermetic or semi-hermetic screw type expander. A design procedure for a reciprocating piston expander for ORC-based power units is proposed in [23]. It allows to estimate the required displacement and assess the feasibility of the single-stage expansion. In [23] the adoption of multi-cylinder architectures is taken into account to limit the expander dimensions. A new concept of reciprocating machine called "nozzle steam piston expander" was also studied [24]. With respect to a conventional piston expander, the "nozzle steam" type presents a restriction in the midway of the intake pipe. This causes the steam to be "shot" into the piston chamber, generating a pressure impulse which leads to a higher p-V (indicated efficiency) with respect to a conventional piston machine. Another interesting novelty in reciprocating expander is represented by the so called "spatial recuperative" feature, represented by an injection of cold refrigerant during the exhaust stroke. This operation ensures that the cold refrigerant receives heat from the hot surrounding refrigerant, partially liquifying and, consequently, reducing the back pressure during the exhaust process [25]. Compared to traditional reciprocating expander, an increase of torque (50%) and of isentropic efficiency (5–6%) is achieved. Generally speaking, a limited volumetric capacity is observed considering that the revolution speed can't be significantly increased. Vibrations and other operational critical aspects occur.

Sliding rotary vane expanders (SVRE) have lower cost, easier manufacturing and simpler structure with respect to other volumetric technologies [26]. An advantage is certainly the good efficiency curve over a wide range of operating conditions, the capacity to deal with two phase working fluids [14] and higher operating pressures [27]. The degree of freedom given by geometry shaping allows to make choices which can recover the volumetric and mechanical efficiency defeats. In fact, these devices suffer in terms of volumetric losses, which contribute even more than friction, to efficiency reduction ([28,29]). In particular, the radial clearance has the greatest impact on expander performance if the blades are not in contact with the stator surface at seal arc [30], or in the case of insufficient lubrication, which produces mechanical losses due to friction. Similarly to other volumetric expanders, an important limit is the reduced expansion ratio (volume ratio during discharging and filling), which prevents the achievement of a complete quasi-adiabatic expansion and, more generally, higher performances when the operating conditions vary [31]. In order to overcome this problem, in [9] a variable expansion ratio was presented and analyzed. The expansion ratio, according to the operating condition, was modified acting on the outlet opening angle. At low load, the expansion ratio passes from 3 to 2, producing an output power and efficiency up to 62% and 56%, respectively.

In previous work, [32], the Authors presented a novel technology suitable to enhance the SVRE performance and operability: it was based on an additional intake port positioned after the main one. The resulting machine has been referred as Dual Intake Port expander (DIP). It was observed that this addition on a conventional SVRE expander leads to an increase of aspirated mass flow rate and, consequently, to a higher produced mechanical power, if the intake and exhaust pressure are kept constant. This is due to the higher permeability of the dual-intake machine (defined as the ratio between the working fluid mass flowrate and the pressure difference between intake and exhaust) with respect to the Single Intake Port (SIP) one. The experimented DIP was made modifying a pre-existing SIP with the main goal to extend the original flow rate operating range for which the SIP machine was designed. This feature appears to be interesting mainly in the transportation sector where the eventual excess of heat on the exhaust gases (or on the other thermal streams) can be furtherly recovered, avoiding wasting it.

At that stage [32], the DIP machine was not conceived as a design option in order to exploit the benefits already observed from a simple modification of an existing SIP machine. Indeed, the higher permeability achieved with the adoption of the DIP option, leads to an intake pressure reduction when machine geometry and the mass flow rate were the same. In fact, the maximum pressure of an ORC-based power unit is definitively fixed by the flow rate produced by the pump: the permeability of the circuit "seen" by the pump fixes the pressure at the pump outlet and expander inlet [33]. This permeability, for a given choice of all the other components, is sensibly influenced by that of the expander: the DIP technology produces a strong permeability increase with a resulting pressure decrease at the expander inlet.

A pressure decrease, for a fixed working fluid flow rate, ensures the improvement of volumetric and mechanical efficiency and the reduction of size and weight of the expander. Nevertheless, the intake pressure reduction can exert a detrimental effect on the produced mechanical power with respect to the SIP, even though during the second fluid filling the pressure inside the vane is increased, recovering power in the indicated form. All these aspects invite to reconceive the design of the expander according to the option of a dual-intake port.

The development of a new design concept of a SVRE considering the DIP technology is the principal aim of this work. The study starts from the experimental comparison between DIP and SIP expander with the same geometry fed by the same mass flow rate. The two expanders have been tested in an ORC-based power unit fed by the exhaust gases of a 3 L supercharged diesel engine (IVECO F1C Engine). The experimental results allow to widen the knowledge about the different thermo-fluid-dynamic behavior of SIP and DIP when the mass flow rate entering them is the same. Furthermore, the collected experimental data acted as a base to validate a theoretical model of the DIP expander, in which additional and more complex thermal and fluid-dynamic phenomena occur. This original validation allowed to use the model to integrate and complete the preliminary vane design optimization of DIP developed through an analytical procedure in order to ensure the same SIP intake pressure and consequently recover the expected mechanical power decrease (with respect to SIP) for a given working fluid flow rate. This issue determined the need for an optimization of the vane dimension and the aspect ratio of the machine (diameter-to-length ratio) which was defined in order to minimize the friction losses. The outcome of this DIP design optimization procedure was compared through the numerical model with the original DIP and SIP machine and also with a retrofitted SIP expander to assess the benefits of a novel design concept based on dual intake port adoption.

2. Experimental test bench

An ORC-based test bench fed by the exhaust gases of a three liters supercharged diesel engine (IVECO F1C) was developed in several previous works by the Authors ([32,33]) in order to assess the theoretical knowledge on the matter, testing different HRVGs and expanders at different operating conditions. In a nutshell, an engineering conclusion is that a great difference has to be expected between theoretical and experimental results when the recovery units are below 5 kW: an experimental phase is mandatory. As working fluid, in this study, R236fa was used, in order to compare the results obtained with the previous experimental campaign reported in [32,33]. The initial choice was also due to the similarity in the thermophysical properties with R245fa which is widely used in this kind of applications. An ISOVG 68 POE oil was mixed inside the working fluid to lubricate the machines. Its amount is equal to 5% of the entire working fluid mass. This oil presence is particularly suitable to improve volumetric and mechanical efficiency of the SVRE used. The main components of the ORC plant reported in Fig. 1 were the following:

- a gear pump driven by an asynchronous electric motor on which an inverter was installed to vary its revolution speed and consequently the mass flow rate provided by the pump;
- a plate and fins heat recovery vapor generator which was conceived to reduce engine backpressure (gas side);
- a sliding rotary volumetric expander (SVRE) which drives an

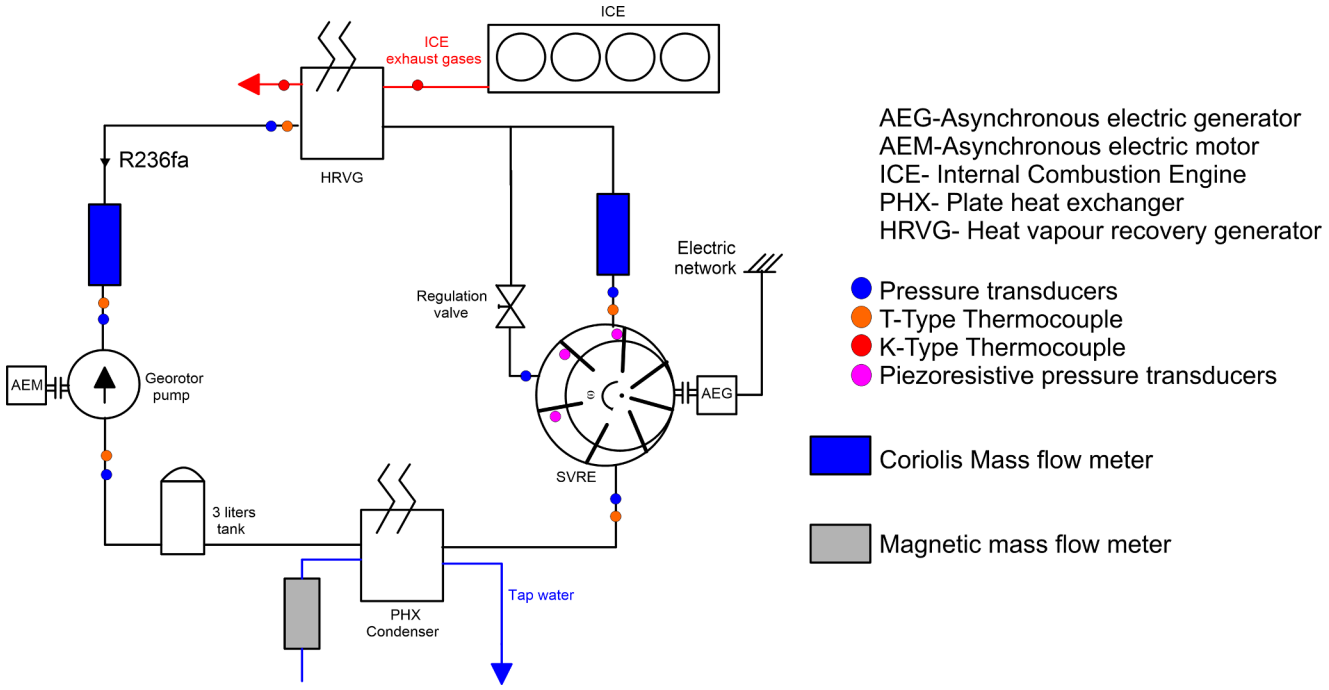

Fig. 1. Experimental ORC based power unit test bench.

asynchronous electric generator connected to the electric grid. For this reason, it was constrained to rotate at 1500 RPM. This solution was adopted because at this step of the study the main goal was the comparison of SIP and DIP keeping constant the operating parameter and consequently the expander revolution speed. Indeed, for a given expander its revolution speed together with the pump speed (and consequently the mass flow rate entering the expander) set the intake pressure inside the vane, [33]. Hence, in order to assess the performance variation due only to the machine architecture, these operating parameters were kept constant. Nevertheless, being the automotive sector the final application of these technological solutions and considering that the revolution speed can be considered as an effective control parameter of the recovery unit, a further comparison between the machines should be performed for different expander revolution speeds. From an operational point of view, this can be done by means of an inverter on the electric machine working also when it behaves like a generator. Moreover, in this study the connection to an electric network operating at 50 Hz was done for sake of simplicity, considering as primary use of the mechanical energy recovered a direct conversion into electric energy and a storage of it in a DC form inside a battery. The driving of the auxiliaries was the first goal following the electrification tendency of them, but a direct use of the mechanical energy as a propulsion aid is also possible, [6].

- a plate heat exchanger condenser cooled by tap water;
- a 3 L tank installed between condenser and pump to dump mass flow rate pulsations and continuously supply the working fluid to the pump, avoiding the occurrence of cavitation at the pump inlet and a continuous and safe feeding.

Fig. 1 shows also the adopted measurement instruments and location. In particular, upstream and downstream each component, pressure transducers and T-type thermocouples were installed to reproduce the T-s cycle thus characterizing the whole real thermodynamic cycle. In order to assess the thermal power recovered from the exhaust gases, K-type thermocouples were located at HRVG inlet and outlet while the exhaust gas mass flow rate was collected from the electronic control unit of the engine. Furthermore, to measure the expander and pump torques and revolution speeds, two torque meters were installed on their shafts. Finally, to reproduce the indicated cycle of the expander, three piezo-resistive sensors were mounted on the lateral covers of the machine, angularly spaced in order to have a suitable overlap. Thanks to these sensors, the indicated power, fundamental to reproduce the intimate behavior of the expander, has been measured. Indeed, from the indicated power and from the mechanical power and shaft speed measured by the torque meter, the volumetric and mechanical efficiency can be assessed [32]. In Table 1 more details on the experimental instruments adopted and their precision were reported.

The experimental campaign was carried out firstly for the SIP expander. In the end of it a second port was added on the same machine and the experiments repeated. This was easily done through the opening of a valve in an auxiliary pipe connected to the exit of the

Table 1
Precision of measurement instruments adopted.

Sensor Type	Measured quantities	Uncertainty
Torque meter	Torque	± 0.02 Nm
	revolution speed	± 1 RPM
Coriolis Flow Meter	Working fluid mass flow rate	± 0.5% of measured value
Magnetic Flow Meter	Water mass flow rate	± 0.5% of measured value
T-type thermocouple	Working fluid temperature	± 0.3 K
K-type thermocouple	Exhaust gases temperature	± 0.4 K
Static pressure sensor	Working fluid pressure	± 0.3 bar
Piezo-resistive sensor	Indicated cycle	± 0.1% of the Full-Scale Sensor Output

Table 2
Geometry values of the expanders.

Stator Diameter d_{stator} [mm]	75.9
Rotor diameter d_{rot} [mm]	65
Eccentricity *ecc* [mm]	5.45
Expander height W_{exp} [mm]	60
Blade length L_b [mm]	17
Blade tick Tk_b [mm]	3.96
Intake port opening angle $\theta_{main\ int,\ start}$ [deg]	4.4
Intake port closing angle $\theta_{main\ int,\ end}$ [deg]	48
Dual Intake port opening angle $\theta_{dual\ int,\ start}$ [deg]	93
Dual Intake port closing angle $\theta_{dual\ int,\ end}$ [deg]	107
Exhaust port opening angle $\theta_{dual\ int,\ start}$ [deg]	180
Exhaust port closing angle $\theta_{dual\ int,\ end}$ [deg]	322.5

HRVG, which guaranteed, at the second port, the same intake temperature and pressure conditions of the main port. This valve was also used to regulate the mass flow rate entering the expander through the second port. Thus, the DIP and SIP expanders were tested making reference to the same machine whose geometry is reported in Table 2 and Fig. 2.

The main intake port and exhaust port are respectively radial (on the cylindrical surface of the stator) and axial (on the cover). The second intake port was placed again radially with an area of 72.35 mm^2. As Table 2 and Fig. 2 show, it was located in an angular position which ensures that when the expander ends the main intake phase, the second one immediately starts. The difference between the dual intake opening angle $\theta_{dual\ int,\ start}$ and main intake closing angle $\theta_{main\ int,\ end}$ was indicated as $\Phi_{dual\ int}$. Being the number of the vanes 7, the vane angle $\Delta\theta_{vane}$ is equal to 51.4°.

3. Experimental comparison between SIP and DIP expanders for a given mass flow rate

3.1. Expander performances and indicated cycle comparison

The benefits introduced by the dual-intake port on the sliding vane expander were fully analyzed in [32], keeping constant the intake and the exhaust pressure. The main advantage is the increase of the machine permeability (Eq. (1)), defined as the ratio between the working fluid mass flowrate $\dot{m}_{wf}$ and the intake pressure p_{in}, which ensures that the machine elaborates a larger mass flow rate, for the same pressure difference between intake and exhaust:

$$\alpha = \frac{\dot{m}_{WF}}{p_{in}} \tag{1}$$

In this way, the expander is able to produce a greater power, enhancing its operability and that of the whole recovery unit. Indeed, this involves the possibility to run a greater mass flow rate of the working fluid. However, the beneficial effects of the higher permeability due to the DIP option can be also used keeping constant the mass flow rate aspirated by the two machines. In particular, to elaborate the same mass flow rate $\dot{m}_{WF}$, the DIP expander produces a much lower intake pressure. In reality, this lower pressure occurs spontaneously at the suction side of the expander, when the pump processes the desired fluid flow rate. This was clearly shown in Fig. 3 which reports the comparison of the measured indicated cycles of the SIP and DIP machine, at a fixed mass flow rate $\dot{m}_{WF}$ of 0.13 kg/s in similar upstream and downstream thermodynamic conditions (Table 3). As it can be noticed from this figure DIP and SIP expanders, for the same aspirated mass flow rate, exhibit different intake pressures, lower in the first case. Main reason was because only a part of the mass flow rate enters the expander through the main intake port ($\dot{m}_{WF,main}$). Since the pipes connecting the HRVG with the expander have the same diameters, the expander is mostly filled by the second intake port ($\dot{m}_{WF,dual\ int}$) due to the lower vane pressure during filling (Fig. 3). According to this behavior, for a given $\dot{m}_{WF}$ produced by the HRVG, the intake pressure can be highly reduced by the presence of the second port. Therefore, in order to regulate the intake pressure, the mass flow rate entering the machine through the dual port should be controlled. This goal can be achieved through a regulation valve (Fig. 4) which reduces the section area of the adduction line which connects the expander dual port with the evaporator.

It can be seen how the presence of the DIP causes the decrease of the intake pressure because the mass flow rate entering the expander at the first intake port diminishes. This causes a reduction of indicated power P_{ind} (Eq. (2)) of DIP (650 W) with respect to the SIP one (816 W).

$$P_{ind} = \frac{\int_{i=1}^{N_v} p_i dV_i}{t_{cycle}} \tag{2}$$

In Eq. (2) p_i and V_i are the pressure and volume values inside the vane, N_v the vane number and t_{cycle} the period of a full rotation of the rotor. Indicated power reaches 623 W for the DIP expander and 816 W for the SIP version.

$$\eta_{vol} = \frac{\dot{m}_{in}}{\dot{m}_{WF}} = \frac{N_V V_{int,end} \rho_{int,end} \omega}{\dot{m}_{WF}} \tag{3}$$

Concerning the volumetric efficiency η_{vol}, it is evaluated in Eq. (3) as the ratio between the theoretical working fluid mass flowrate inside the vane in the end of the intake phase ($\dot{m}_{in}$) and the real one ($\dot{m}_{wf}$). In particular, the first can be evaluated though the vane number N_v, the rotational speed ω, the vane volume in the end of the filling process ($V_{int,end}$) and the related working fluid density ($\rho_{int,end}$), considering an isothermal process. DIP machine has a $\eta_{vol,}$ equal to 58.3%, higher than that obtained by SIP (42%). This happens for two reasons:

1) the DIP machine works with a lower intake pressure p_{in}, so, as the exhaust pressure p_{exh} is quite equal for the two expanders, the pressure difference Δp_v between adjacent chamber decreases. Indeed, Δp_v is the main driver of the leakages at tip-blade which is the most important volumetric loss.
2) the DIP introduction provides an extension of the intake phase and a reduction of expansion one with respect to SIP expander; so, the pressure is kept constant for a wider angular extent Δθ (Fig. 3). This ensures that the Δp_v with adjacent vanes (which can be observed comparing the corresponding indicated cycles phased in the sense of rotation) takes place for a narrower Δθ in DIP expander.

Moreover, the indicated efficiency η_{ind}, evaluated in Eq. (4) as the ratio between indicated power and the power produced in adiabatic isentropic condition, is higher for the dual-intake expander. In this case η_{ind} is 45.7% for the DIP against the 39.6% achieved in the SIP.

$$\eta_{ind} = \frac{P_{ind}}{\dot{m}_{WF}(h_{in} - h_{out,is})} \tag{4}$$

Therefore, the experimental comparison showed that DIP has a lower intake pressure than SIP in the same operating conditions producing higher volumetric and indicated efficiency and a lower indicated power. This means that despite DIP allows to work in more efficient conditions from a thermodynamic point of view, its design should be reconceived to overcome the power gap when the $\dot{m}_{WF}$ entering the machine is the same of SIP.

3.2. Analysis of mechanical efficiency

Given these results, the authors performed a further study on the mechanical power on the shaft P_{mech}. For such machine, the mechanical power is quite exclusively lost because of the dry friction related to the relative motion of the blades on the stator inner surface. Thus, P_{loss} can be evaluated through Eq. (5):

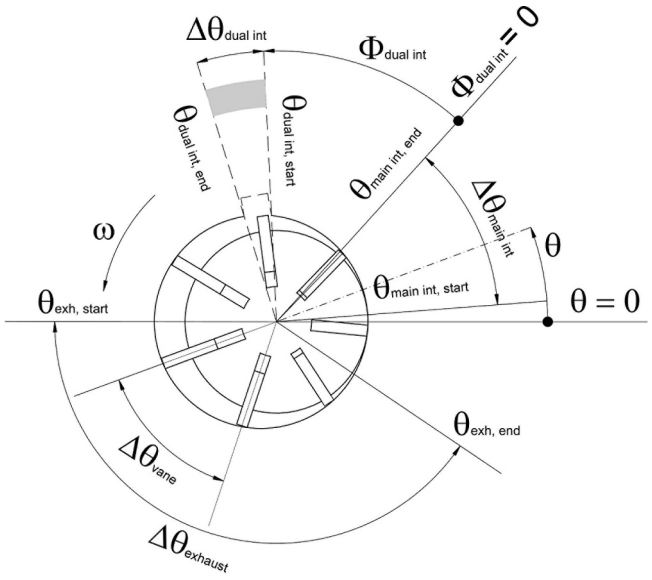

Fig. 2. Single SIP and dual intake DIP expander.

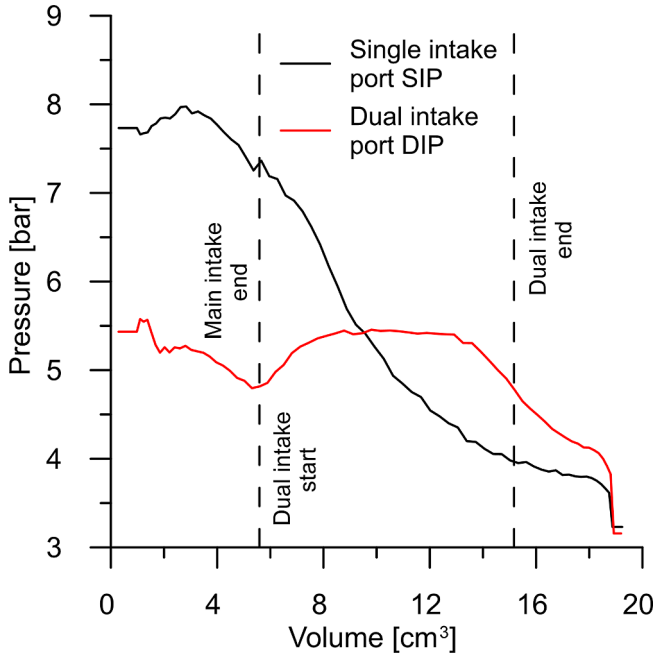

Fig. 3. Single SIP and dual intake DIP expander indicated cycle keeping constant the elaborated mass flow rate.

$$P_{loss} = N_v C_{tip} F_n r_v \omega \tag{5}$$

where F_n is the normal force acting on the blade, N_v is the blade number, C_{tip} the friction factor, r_v (Eq. (6.1)) the instantaneous distance between the blade tip and rotor center and ω the revolution speed. F_n is given by the sum of centrifugal force acting on the blade F_c (Eq. (6.2)) and the pressure action exerted by the fluid under the blade F_p (Eq. (6.3)).

$$r_v = ecc \bullet \cos\theta + \sqrt{\left(\frac{d_{stator}}{2}\right)^2 + ecc^2(cos^2\,\theta - 1)} \tag{6.1}$$

$$F_c = m_b \omega^2 \left(r_v - \frac{L_b}{2}\right) \tag{6.2}$$

$$F_p = (p_{rot} - p_{ext,env}) W_b Tk_b \tag{6.3}$$

F_c (Eq. (6.2)) is proportional to the blade mass m_b, rotational speed squared ω^2, and the difference between r_v and half the blade length. So, being r_v (Eq. (6.3)) function of eccentricity (ecc), angular position of the rotor (θ) and stator diameter (d_{stator}) F_c also depends on the expander configuration. Concerning F_p (Eq. (6.3)) it is related to the pressure exerted by the fluid on the blade. In fact, W_b and Tk_b represent the wideness and thickness of the blade respectively. Their product determines the surface on which the pressure difference between p_{rot} and $p_{ext,end}$ acts. The difference between theese absolute pressures (p_{rot} and $p_{ext,env}$) represents the relative pressure of the fluid under the blade with respect to the environment outside the machine. For the case considered $p_{ext,env}$ is the atmospheric pressure so it is kept equal to 1 bar. Thus, as it can be observed from the reported equations, the whole friction contribution depends on the expander geometry, dry friction coefficient C_{tip}, pressure under the blade p_{rot} ($p_{ext,env}$ is constant) and revolution speed ω. If the machines have the same geometry, materials and were tested under the same operating conditions they have the same C_{tip} so it is theoretically expected that DIP has a lower P_{loss} than SIP. This happens because while F_c is equal for both machines, F_p diminishes due to the p_{rot} reduction. Indeed, as experimentally observed, p_{rot} depends on the intake pressure which is lower in DIP.

The lower P_{loss} ensures that DIP has a higher or at least a comparable mechanical efficiency η_{mech} depending on how much p_{rot} of DIP is higher than the SIP one and the impact of P_{loss} on P_{ind}. Indeed, η_{mech} was expressed as the ratio of P_{mech} and the indicated power P_{ind} as in Eq. (7).

$$\eta_{mech} = \frac{P_{mech}}{P_{ind}} \rightarrow \eta_{mech} = \frac{P_{ind} - P_{loss}}{P_{ind}} \rightarrow \eta_{mech} = 1 - \frac{P_{loss}}{P_{ind}} \tag{7}$$

Nevertheless, the experimental comparison in terms of mechanical power reported in Table 3 indicates that DIP has lower P_{mech} and η_{mech} (367 W and 58.9%) with respect to the SIP (650 W and 79.6%). However, as the machine geometry and components material were the same in the two cases as well as the revolution speed, the difference from the theoretical expectation can be only due to a different friction factor C_{tip} between blade tip and stator, which is the main contribution to the friction power lost. After a thorough analysis of the machine, it was seen that this C_{tip} difference was caused by the wear of the dual-intake port expander produced by the long working of the machine when it had only a single-intake port. Indeed, the C_{tip} of SIP is equal to 0.01 while the one of DIP is equal to 0.05. Both these values were obtained through a calibration procedure of the respective GT-Suite™ models considering that C_{tip} cannot be measured and it is difficult to theoretically predict as the blades are not in permanent contact with the stator inner surface for the hydrostatic lubrication of the oil and the undesired phenomenon called “blade chatter” [29]. The C_{tip} of SIP was obtained from the model calibration developed by the authors in [33] while the DIP C_{tip} through the calibration of an updated version of the model developed in [32] which will be furtherly discussed in Section 4. However, if there is no wear of the components and the machines are the same, the C_{tip} can be considered equal for the two devices. For this reason, in the following theoretical and numerical comparisons between SIP and DIP, C_{tip} was kept constant at 0.01.

Hence, DIP can theoretically reach higher η_{ind} and comparable η_{mech}

[1] In order to consider the effect of this sudden expansion (which always happens in volumetric machines), it should be noticed as Eq. (8) is not completely suitable to describe the expander efficiency η_{exp}. In fact, the denominator of Eq. (8) should be referred to the achievable maximum expansion work which is not the isentropic one in volumetric machines (as it happens in dynamic machines). To simplify the efficiency definition, the overall scientific literature doesn’t consider this aspect and always makes reference to an isentropic ideal transformation but an error is introduced. A more suitable definition should be defined which considers that if the vane pressure at exhaust opening is higher than the outlet pressure, an isochoric expansion takes place and an ideal isentropic (quasi-adiabatic) expansion can’t be achieved.

Table 3
Comparison between single and dual intake expander performance keeping constant the elaborated mass flow rate

Operating condition	Single Intake Expander SIP	Dual Intake Expander DIP
Intake pressure p_{in} ± 0.3 [bar]	7.7	5.93
Intake Temperature T_{in} ± 0.03 [°C]	75	70
Elaborated mass flow rate m_{wf} ± 0.5% [kg/s]	0.130	0.130
Exhaust pressure p_{exh} ± 0.3 [bar]	3.23	3.16
Expander performance	Single Intake Expander SIP	Dual Intake Expander DIP
Indicated Power ± 2% P_{ind} [W]	816.2	622.5
Mechanical power P_{mech} ± 0.8% [W]	650	367
Mechanical Efficiency ± 2.8% η_{mech} [%]	79.6	58.9
Volumetric Efficiency ± 2.3% η_{vol} [%]	42	58.3
Indicated Efficiency ± 2.5% η_{ind} [%]	39.6	45.7
Global efficiency ± 1% η_{glob} [%]	31.5	27

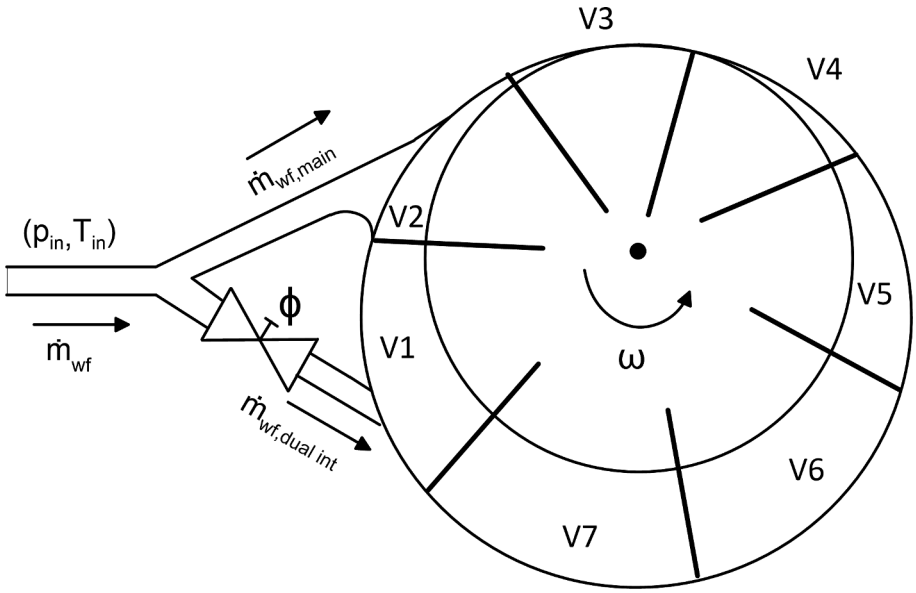

Fig. 4. Scheme of the DIP system and the regulation valve on the pipe feeding the second intake port.

with respect to SIP. Consequently, being the whole expander efficiency η_{exp} the product of η_{mech} and η_{ind} (Eq. (7)), DIP allows to enhance η_{exp}.

$$\eta_{exp} = \frac{P_{mech}}{\dot{m}_{WF}(h_{in} - h_{out,is})} = \frac{P_{ind}}{\dot{m}_{WF}(h_{in} - h_{out,is})} \cdot \frac{P_{mech}}{P_{ind}} \quad (8)$$

It is worth noting how in Eq. (8), the adiabatic-isentropic expansion was considered as the reference transformation. Indeed, h_{in} is the specific enthalpy at expander inlet while $h_{out,is}$ is the specific enthalpy at expander outlet in isentropic condition.

4. Numerical model and experimental validation

4.1. Structure of numerical DIP model

In order to deepen the understanding of the DIP behavior, a GT-Suite™ numerical model was used refining a model developed by the authors in [32]. In Fig. 5, the structure of the model was shown, focusing on the boundary conditions introduced at the intake ($\dot{m}_{WF}$ and T_{in}) and exhaust side (expander exhaust pressure p_{exh}). The unknown quantities are $p_{main,int}$, $p_{dual\ int}$, $\dot{m}_{WF,main}$, $\dot{m}_{WF,dual\ int}$, respectively the pressures and the mass flow rates at main and secondary intake ports. The model allows also to evaluate the indicated power P_{ind} (Eq. (2)), the power loss due to friction effects P_{loss} (Eq. 6) and, finally, the mechanical power P_{mech} on the shaft. Flow leakages between rotor faces and casing ("1", in Fig. 5), at vane tip ("2", in Fig. 5), vane side ("3", in Fig. 5) and have been calculated too through the approach of equivalent orifice nozzles [34]. More details on the general structure of the model are not reported in this work for the sake of brevity and they can be found in [32].

The DIP model was validated through data reported in Table 4 for different openings ϕ (defined as the ratio between the restricted section area and the open one) of the valve with the aim of using it as a design software platform. In particular, in Table 4 cases 1, 2, 3 represent the fully open pipe (ϕ = 100%) while cases 4, 5, 6 have ϕ values respectively equal to 60%, 50% and 45%. $p_{int,main}$ varies in a range between 5.3 bar and 6.4 bar, close to $p_{dual\text{-}int}$ values when the second port is fully opened (case 1, 2, 3).

When ϕ = 100%, $\dot{m}_{wf,dual\text{-}int}$ is higher than $\dot{m}_{wf,main}$ representing 60% of the mass flow rate coming from the HRVG. When ϕ decreases (cases 4, 5, 6), $\dot{m}_{wf,dual\text{-}int}$ decreases too, causing a $p_{int,main}$ increase and a $p_{dual\ int}$ decrease. This can be observed, comparing case 1 and case 5 which have different ϕ, but elaborates the same overall mass flow rate $\dot{m}_{WF}$. Indeed, this comparison shows that, when ϕ decreases from 100% (case 1) to 50% (case 5), $\dot{m}_{wf,dual\text{-}int}$ decreases from 0.080 kg/s to 0.059 kg/s ensuring a $p_{int,main}$ increase from 6.1 to 6.4 bar and a $p_{dual,int}$ decrease from 5.7 to 5.4 bar, in accordance with the expectations.

This contributes to enhance the mechanical power P_{mech} which raises from 304 W to 398 W. However, the P_{mech} increase was not only due to the ϕ decrease but also to the lower p_{exh} (see case 5). Concerning other cases, the expander with a DIP option partially closed shows always a higher P_{mech} with respect to cases in which ϕ = 100%. In fact, for cases 1–3, P_{mech} varies from 263 W to 304 W while for cases 4–6 it ranges from 323 W to 398 W. On the other hand, the volumetric efficiency decreases when ϕ is reduced from an average value close to 60%

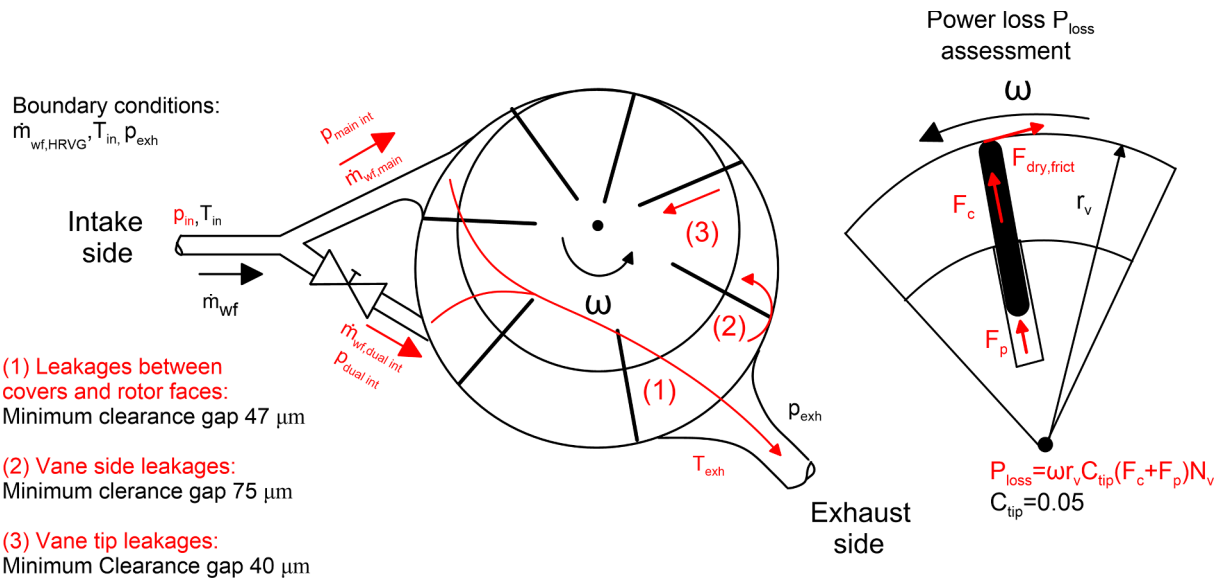

Fig. 5. Structure of the DIP expander model. Boundary conditions are: $\dot{m}_{WF,HRVG}$, T_{in} and p_{exh}. Quantities to be calculated: $p_{main,int}$, $p_{dual\ int}$, $\dot{m}_{WF,main}$, $\dot{m}_{WF,dual\ int}$, flow leakages and indicated P_{ind} and mechanical power P_{mech}.

(cases 1–3) to a value close to 55% (case 4–6). This is due to the intrinsically dissipative nature of the flow regulation which implies a throttling of the second intake. Unlike P_{mech} and η_{vol}, the global efficiency η_{glob} is quite constant, being the variation comprised between 25% and 26% and the main reason of this low value is certainly the low mechanical efficiency (55%–60%).

4.2. Experimental validation

A first important validation was referred to the volumetric efficiency for which the real mass flow rate was measured. It must be equal to the sum of the flowrate entering the vanes and that feeding the leakages whose contribution can be separately evaluated as equivalent nozzles which need coefficients relating pressure difference and flow rates. Three contributions have been outlined: (1) the leakage on the machines covers and rotor surfaces which reports about a fluid quantity which escapes without interfering with the vanes, (2) the leakage among the vanes at tip blade; (3) the leakages which pass through the slots inside the rotor and the blade-side. These contributions require a suitable estimation of the respective clearances which can be only identified comparing the working fluid crossing the machine and the indicated cycle with those measured [33]. The optimum set of clearances which resulted valid for a number of experimental conditions (Table 4 of section 4) is reported in Fig. 5.

The second important validation concerns the mechanical efficiency of the machine which deeply involves: a) the prediction of the indicated cycle; (b) the prediction of the mechanical losses due to friction. Indicated cycle – as already discussed – is closely related to the fluid inside the vanes and, consequently, to the volumetric behavior of the machine. The good prediction reported in Fig. 6 allows to be confident with real processes. Indeed, Fig. 6 shows how the model is able to reproduce the real DIP indicated cycle. Only when the vane volume is equal to 5 cm^3 a slight difference between the experimental and numerical trend was observed. This is due to the more complex phenomena taking place for this volume when the main intake port is closing and the dual intake one is opening. So, the model is not completely able to represent this transition: the experimental trend shows a higher pressure drop than that predicted by the model which clearly neglect some secondary phenomena which are always dissipative. However, this aspect does not affect the reliability of the model which allows a good general representation of the indicated cycle as can be seen also by the Root Mean Square Error RMSE between the real and predicted data (Fig. 6). Friction losses, on the other hand, require the identification of the friction coefficient – Eq. (5) – and this implies the knowledge of the mechanical power (torque & speed of revolution) measure on the shaft, being the other variables in Eq. (5) predictable from the comprehensive modelling of the machine which evaluates also the motion of the blades inside the slots and, therefore, the real and

Table 4
Experimental quantities of dual intake expander.

	1	2	3	4	5	6
ϕ	100%	100%	100%	60%	50%	45%
ω ± 1 RPM	1516.6	1513.8	1512.3	1517.8	1520.9	1520.7
$\dot{m}_{wf,main}$ ± 0.5% [kg/s]	0.049	0.046	0.044	0.061	0.071	0.069
$\dot{m}_{wf,dual\text{-}int}$ ± 0.5% [kg/s]	0.080	0.073	0.067	0.070	0.059	0.050
$p_{int,main}$ ± 0.3 [bar]	6.1	5.6	5.3	6.4	6.4	6.0
$p_{,dual\text{-}int}$ ± 0.3 [bar]	5.7	5.4	5.1	5.6	5.4	4.7
p_{exh} ± 0.3 [bar]	3.6	3.3	3.1	3.6	3.2	3.0
T_{in} ± 0.03 [°C]	78.9	70.4	77.2	79.5	78.9	64.7
T_{exh} ± 0.03 [°C]	72.8	63.4	71.2	71.9	70.2	54.9
P_{ind} ± 2% [W]	535	507	469	565	639	541
P_{mech} ± 0.8% [W]	304	270	263	323	398	329
η_{vol} ± 2.3% [%]	59	60	59	57	55	57
η_{mech} ± 2.8% [%]	57	53	56	57	62	61
η_{glob} ± 1% [%]	26	25	26	25	25	25

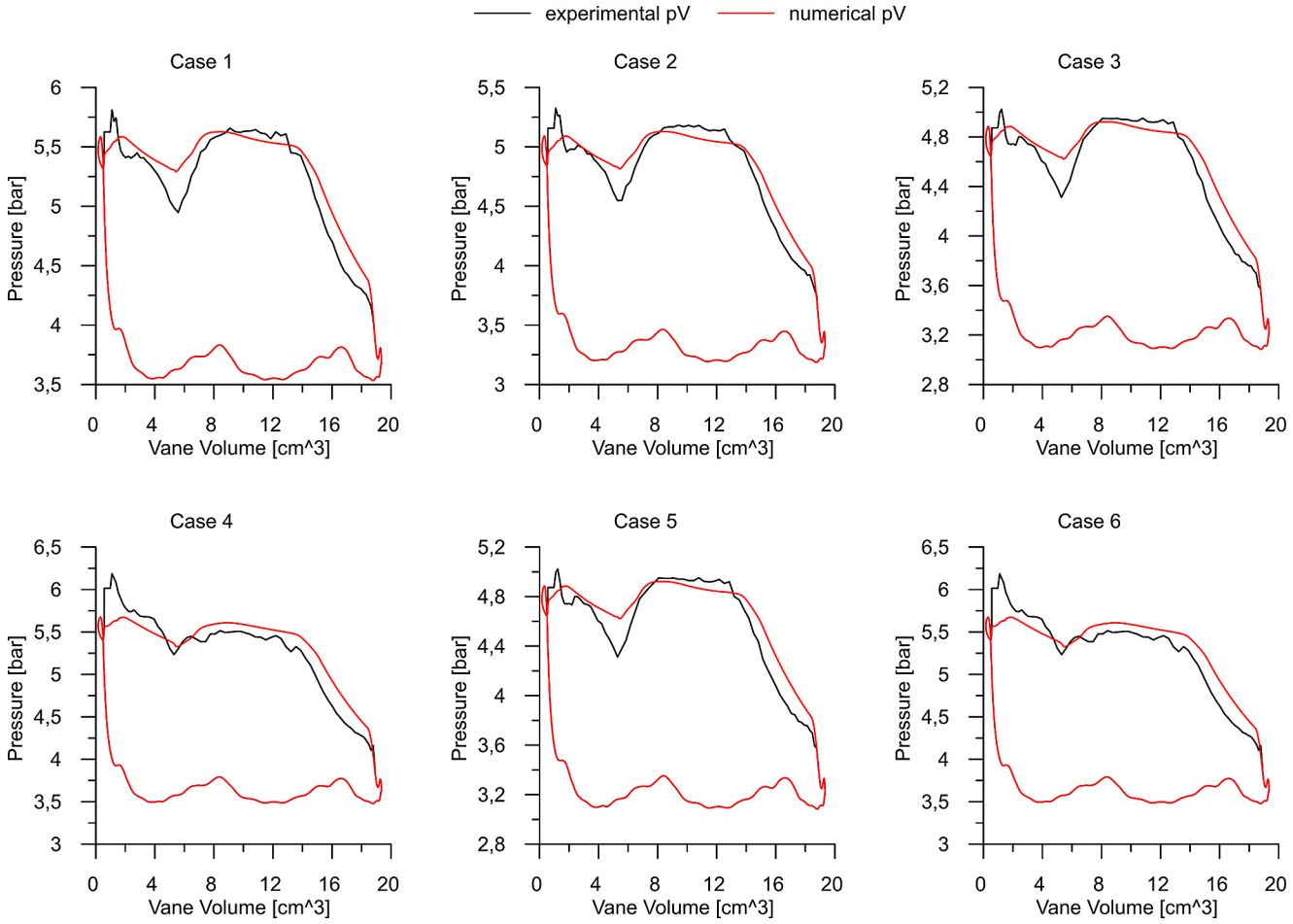

Fig. 6. Comparison between experimental and numerical indicated cycle. From left top to right down, RMSE is 2.6%; 2.7%; 2.5%; 3.7%; 5.0%; 4.9%.

inertial forces acting on them. Therefore, after the calibration process, the C_{tip} was found to be equal to 0.05. Once the model calibration was performed, the predicted data were compared with the experimental ones showing lower absolute relative errors and RMSE as it can be observed from Table 5. In particular RMSE on $\dot{m}_{wf,main}$, $\dot{m}_{wf,dual\text{-}int}$, $p_{int,main}$, $p_{dual\text{-}int}$, P_{ind}, P_{mech} are 2%, 1.9%, 0.6%, 1.3%, 3.6%, 2.4% respectively. Thus, as a result of the validation process, the model can be considered highly reliable in reproducing the real phenomena taking place inside the expander.

In order to support the use of the platform as a design tool, a preliminary pre-design phase was needed in order to orient the design of a DIP machine. In this case, in fact, the condition that the DIP machine operates with the same inlet pressure of the SIP producing a comparable P_{mech} is mandatory for a desired same mass flow rate. Moreover, a choice on the aspect ratio (length & diameter) of the machine still appear useful. Aspect ratio represents an interesting degree of freedom in the design of a SVRE. For an acceptable minimum clearance, it defines the cross-sectional areas of the fluid leakages affecting the volumetric efficiency of the machine. “Disk” or “finger” shaped expanders have quite different blade geometry and different relative velocities among fixed and rotating components which determines quite a difference on mechanical efficiency too. Therefore, an analytical model was developed in order to deal with a preliminary pre-design of the expander.

5. Fully theoretical analytical model of dual-intake SVRE

5.1. Structure of theoretical model

The experimental comparison reported in Table 3 shows that the DIP expander produces a lower mechanical power P_{mech} with respect to the original machine when the mass flow rate coming from the evaporator $\dot{m}_{wf}$ is the same. This is due to the fact that this expander was originally conceived as a SIP expander and simply modified opening a second port. In any case, the DIP machine realized this way demonstrated some intrinsic advantages such as the higher η_{vol} and η_{ind} with respect to a conventional SIP machine suggesting the need for further improvements.

Therefore, with the aim to develop a dual-intake machine alternative to the conventional one, the SVRE must be re-designed: the vane geometry is the preliminary parameter to be chosen, being more than one vane responsible of the flow rate inducted by the machine (as it happens for the SIP machine). Moreover, when defining the vane geometry, the aspect ratio of the machine is certainly the most important parameter. A pre-set up of this parameter, before the application of the fully comprehensible software platform, is certainly needed.

A theoretical model able to pre-design the vane volume of a DIP machine, which ensures the same flow rate aspirated by a SIP machine,

Table 5
Absolute relative error between predicted and experimental values.

Cases	1	2	3	4	5	6	RMSE
$\dot{m}_{wf,main}$	6.8	5.2	3.3	4.2	0.9	4.5	2.0
$\dot{m}_{wf,dual\text{-}int}$	4.1	2.9	1.9	3.6	1.0	6.4	1.9
$p_{int,main}$	2.6	2.5	2.6	3.2	1.8	1.4	0.6
$p_{,dual\text{-}int}$	2.9	0.5	0.8	2.7	3.7	2.7	1.3
P_{ind}	1.1	5.5	0.6	0.6	6.7	8.8	3.6
P_{mech}	0.4	2.7	0.8	2.2	1.5	7.0	2.4

keeping the same inlet pressure, has been derived in an analytical form. With this aim, this new modeling widens the validity of a similar model developed for a single vane machine [33]. The condition on the vane geometry, which assures the same intake pressure, is not straightforward and it can be *a-posteriori* verified, but only after a long iterative procedure based on the comprehensive modeling of the machine.

The procedure starts rearranging Eq. (3) to make explicit the working fluid density as a function of $\dot{m}_{WF}$ and η_{vol}, Eq. (9). Then, introducing Eq. (9) in the ideal gas equation (Eq. (10)) corrected by a compressibility factor Z to represent the real gas behavior, Eq. (11) was obtained:

$$\rho_{int,end} = \frac{\eta_{vol}}{N_V V_{int,end}\omega}\dot{m}_{WF} \tag{9}$$

$$\frac{p_{int,end}}{\rho_{int,end}} = ZRT_{in} \tag{10}$$

$$p_{int,end} = \frac{ZRT_{in}(p_{int,end})\eta_{vol}}{N_V V_{int,end}\omega}\dot{m}_{WF} \tag{11}$$

Adding to the right-end-side term of Eq. (11) the contribution Δp_{loss} (pressure losses as a function of $\dot{m}_{WF}$), the expression of the intake pressure p_{in} is derived (Eq. (12)). In fact, due to volumetric losses and vane volume increase during the intake phase, the pressure at the expander inlet p_{in} is higher than that at the end of the intake process $p_{int,end}$. Δp_{loss} can be represented by a linear interpolation of the experimental data [33].

$$p_{in} = \frac{ZRT_{in}(p_{in})\eta_{vol}}{N_V V_{int,end}\omega}\dot{m}_{WF} + \Delta p_{loss} \tag{12}$$

It was demonstrated in [33] that, for a low excursion of T_{in}, the intake pressure grows quite linearly with $\dot{m}_{WF}$, if the expander revolution speed is kept constant. Nonetheless, the development in [33] conceived for a single intake expander can be applied also to a dual intake one, if the dual intake phase starts immediately after the end of the main one. In the DIP machine, this condition applies and the two ports produced a continuous angularly longer fluid induction. So, for what concerns the use of Eq. (12), the new vane volume at dual-intake port closing $V_{dual\ int,end}$ must be considered as $V_{int,end}$. Nevertheless, Eq. (12) allows to represent the global behavior of the expander in terms of lumped relation between intake pressure and mass flow rate, but it doesn't give the distinction between the contributions of the two ports. So, it doesn't outline the effects of $\dot{m}_{WF,dual\ int}$ and $\dot{m}_{WF,main}$ on the expander intake pressure. Hence, in order to fill this gap, the relation between intake pressure and mass flow rate was furtherly investigated for the dual intake case, obtaining a new analytic relation between p_{in} and $\dot{m}_{WF,dual\ int}$ and $\dot{m}_{WF,main}$.

This was done considering the mass inside the vane at the end of the dual intake phase m_v as the sum of $m_{v,main}$ and $m_{v,dual\ int}$ (Eq. (13.1)).

$$m_v = m_{v,main} + m_{v,dual\ int} \tag{13.1}$$

As the second intake starts immediately after the end of the main one, they are not overlapped and can be considered separated. So, Eq. (13.2) applies:

$$\rho_{glob} = \frac{\rho_{main} V_{main,end} + \rho_{dual\ int} V_{dual\ int,end}}{V_{dual\ int,end}} \tag{13.2}$$

where ρ_{glob} is the working fluid density at the end of the whole intake phase (the main and the second) while $\rho_{main,end}$ and $\rho_{dual\ int,end}$ are respectively the working fluid density if the expander was fed only by the main and the dual intake port, not cumulating the two filling effects. In particular, $\rho_{dual\ int}$ represents the working fluid density at the end of dual intake phase if the vane was empty when the dual intake phase starts. This is obviously a theoretical assumption because the vane is filled by the dual intake port only after the end of main one, so, the vane cannot be empty when the dual intake starts. Nevertheless, this assumption is useful to highlight the effects of dual intake port on the overall aspirated mass.

Therefore, extending the validity of Eq. (9) to the case in which two ports feed the expander, the following global density can be expressed (Eq. (14)):

$$\rho_{glob} = \frac{\eta_{vol,main}\dot{m}_{WF,main} + \eta_{vol,dual\ int}\dot{m}_{WF,dual\ int}}{N_V \omega V_{dual\ int,end}} \tag{14}$$

Subsequently, entering Eqs. (14) in Eq. (10) and repeating the passages which allows to outline Eq. (12), the effects of the two flow stream $\dot{m}_{WF,dual\ int}$ and $\dot{m}_{WF,main}$ on the intake pressure can be outlined (Eq. (15)).

$$p_{in} = ZRT_{in}\left(\frac{\eta_{vol,main}\dot{m}_{WF,main} + \eta_{vol,dual\ int}\dot{m}_{WF,dual\ int}}{N_V \omega V_{dual\ int,end}}\right) + \Delta p_{loss} \tag{15}$$

Multiplying and dividing the right-end-side term of Eq. (15) by $\dot{m}_{WF}$, Eq. (16) was obtained:

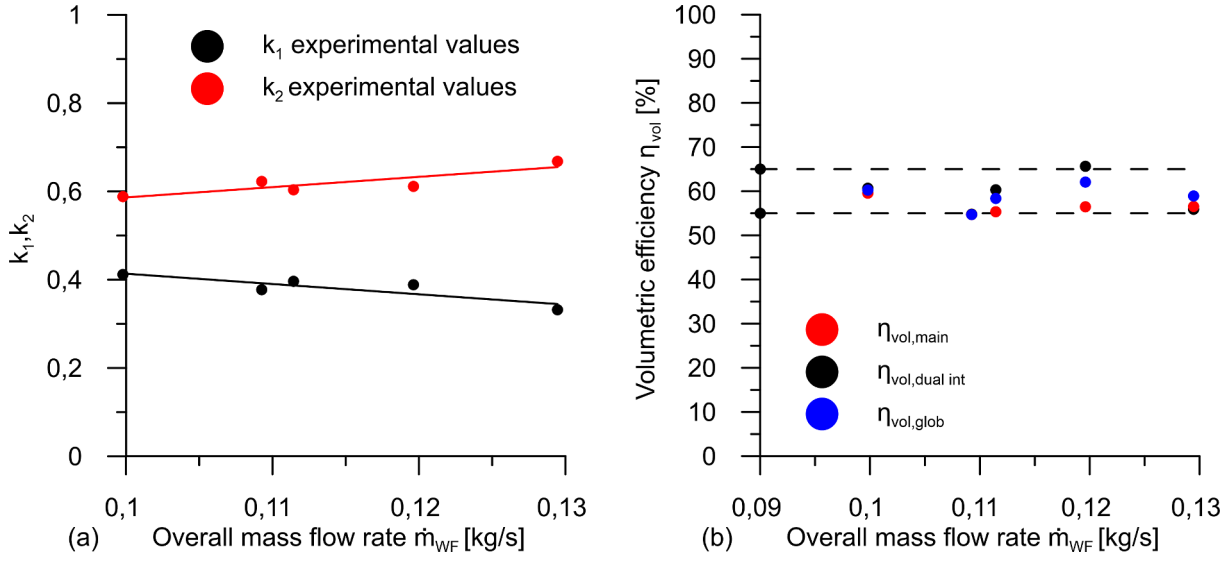

Fig. 7. k_1 and k_2 (a) and $\eta_{vol,glob}$, $\eta_{vol,main}$ and $\eta_{vol,dual\ int}$ (b) variations with $\dot{m}_{WF}$.

$$p_{in} = \frac{ZRT_{in}}{N_V \omega V_{dual\ int,end}}(\eta_{vol,main}k_1 + \eta_{vol,dual\ int}k_2)\dot{m}_{WF} + \Delta p_{loss} \quad (16)$$

where Δp_{loss} was expressed in Eq. (17) as a linear variation with $\dot{m}_{WF}$:

$$\Delta p_{loss} = k'\dot{m}_{WF} + q \quad (17)$$

with k′ and q obtained through the interpolation of experimental data. Concerning k_1 and k_2 (Eq. (18)), they represent the fraction of the overall mass flow rate aspirated by the expander through the main and the second intake port, respectively. They depend by the throttling degree and by the dimensions of the adduction pipes of the two ports.

$$k_1 = \frac{\dot{m}_{WF,main}}{\dot{m}_{WF}}$$
$$k_2 = \frac{\dot{m}_{WF,dual\ int}}{\dot{m}_{WF}} \quad (18)$$

It is worth observing how the combination of Eqs. (9) and (14) allows to represent $\eta_{vol,glob}$ as a function of $\eta_{vol,main}$ and $\eta_{vol,dual\ int}$. Indeed, expressing ρ_{glob} of Eq. (14) as a function of $\eta_{vol,glob}$ (Eq. (9)) and taking into account Eq. (18), Eq. (19) can be written:

$$\eta_{vol,glob} = \frac{\eta_{vol,main}\dot{m}_{WF,main} + \eta_{vol,dual\ int}\dot{m}_{WF,dual\ int}}{\dot{m}_{WF}} = \eta_{vol,main}k_1 + \eta_{vol,dual\ int}k_2 \quad (19)$$

Thus, Eq. (19) represents a weighted average which allows to evaluate the impact on $\eta_{vol,glob}$, of $\eta_{vol,main}$ and $\eta_{vol,dual\ int}$. The weights are represented by k_1 and k_2 i.e. by the repartition among the two ports of the fluid entering the expander.

5.2. Validation of theoretical model

As mentioned before, if the two feeding pipes are equal, k_2 is higher than k_1 because $\dot{m}_{WF,dual\ int}$ is higher than $\dot{m}_{WF,main}$. It was experimentally demonstrated that, for the considered case when ϕ is 100%, the proportion between $\dot{m}_{WF,main}$ and $\dot{m}_{WF,dual\ int}$ linearly changes, showing a small slope with $\dot{m}_{WF}$. In fact, as Fig. 7(a) shows, the experimental values of k_1 and k_2 are almost constant when $\dot{m}_{WF}$ varies from 0.099 kg/s to 0.130 kg/s.

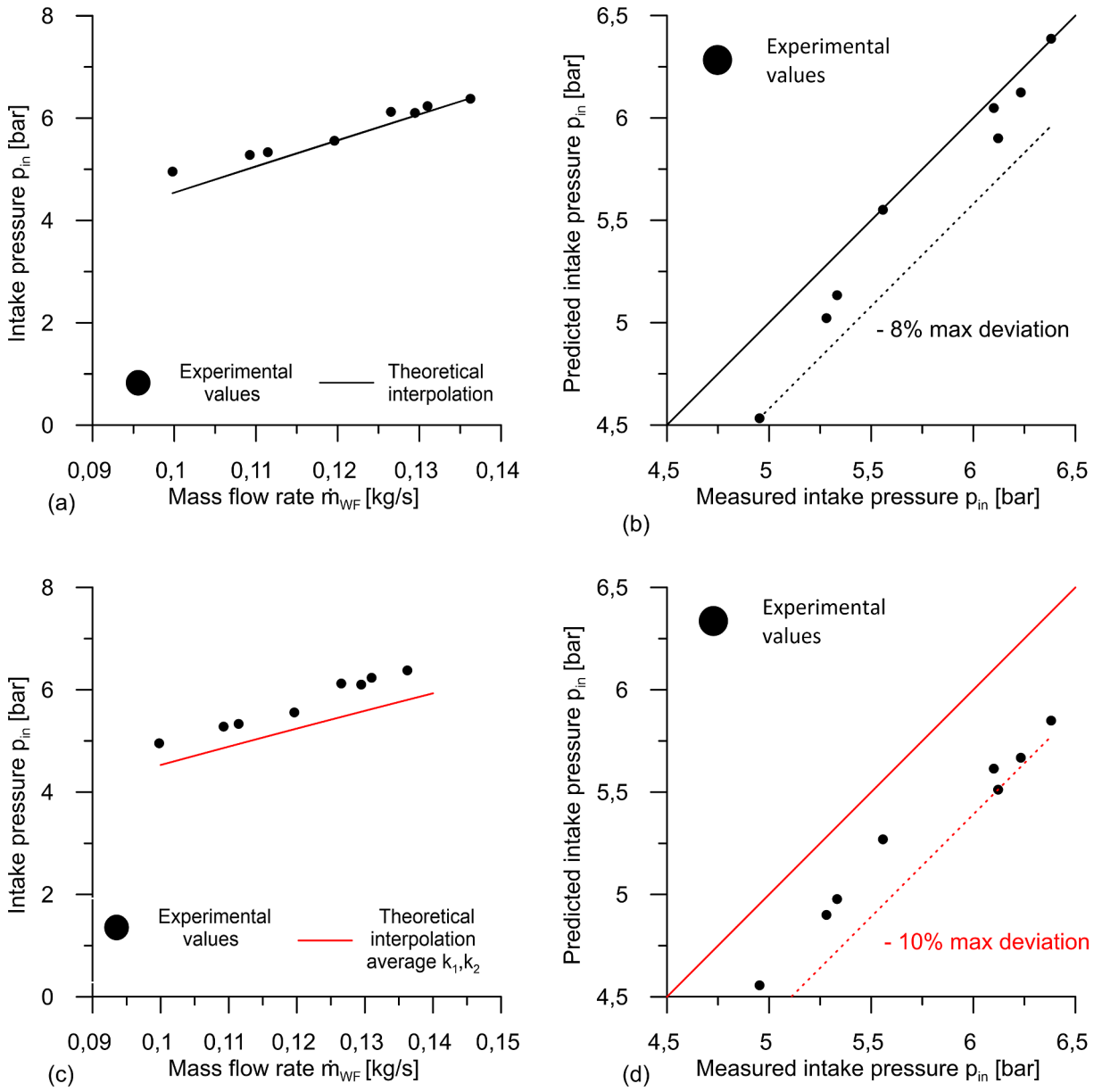

Fig. 8. Theoretical interpolation of experimental intake pressure p_{in} values (a) and deviations between predicted and experimental p_{in} (b). Theoretical interpolation (c) and deviation from experimental data (d) averaging k_1 and k_2.

Moreover, the difference between the three volumetric efficiencies ($\eta_{vol,glob}$, $\eta_{vol,main}$ and $\eta_{vol,dual\ int}$) is small and they slightly depend on $\dot{m}_{WF}$. As a matter of fact, in Fig. 7(b) it can be noticed that the values of $\eta_{vol,glob}$, $\eta_{vol,main}$ and $\eta_{vol,dual\ int}$ are comprised in a range between 55% and 65%. Thus, in Eq. 13, k_1 and k_2 can be represented by a linear law as a function of $\dot{m}_{WF}$ (interpolation of experimental points as done in Fig. 7(a)). Moreover, the weak dependence of $\eta_{vol,glob}$, $\eta_{vol,main}$ and $\eta_{vol,dual\ int}$ with $\dot{m}_{WF}$ can be neglected and average values can be assumed. Nonetheless the introduction of this approximation on k_1, k_2, $\eta_{vol,glob}$, $\eta_{vol,main}$ and $\eta_{vol,dual\ int}$ in Eq. (15), ensures to predict intake pressure values close to the real ones as can be observed in Fig. 8(a). Here, the theoretical estimation fits with a satisfying accuracy the experimental data: the maximum deviation between experimental and predicted values of p_{in} is about 8%, which occurred for the lower value of mass flow rate (Fig. 8(b)). This is a good result considering the assumptions and the relative simplicity of the derivation done.

It is worth observing how k_1 and k_2 show a weak linearity with mass flow rate so it could be reasonable to consider them constant when p_{in} is evaluated (Eq. (16)). In order to assess the error introduced by this assumption, p_{in} evaluation was repeated through Eq. (16) introducing in k_1 and k_2 their average values. In Fig. 8(c) the comparison was reported and, despite the experimental trend was correctly reproduced, the prediction was poorer being the differences between theoretical and measured values greater than those of the original case (Fig. 8(a)) in which k_1 and k_2 are considered linearly variable with the mass flow rate.

This was confirmed by the increase of deviation of the predicted trend from the experimental values (Fig. 8(d)) with respect to the case in which k_1 and k_2 are not averaged (Fig. 8(b)). Moreover, Fig. 8(c) shows that averaging k_1 and k_2, the divergence increases with $\dot{m}_{WF}$, reaching a maximum deviation of 10%. Thus, an average value for k_1 and k_2 can be used for a preliminary evaluation but, for a more detailed analysis, this hypothesis should be removed, mainly for higher $\dot{m}_{WF}$. Indeed, k_1 and k_2 influence the repartition of the mass flow rate among the two ports: even a slight variation of these flow streams produces a not negligible variation on the intake pressure according to Eq. (16).

5.3. Preliminary design of DIP through fully theoretical model and DIP downsizing

The value of $V_{dual\ int,end}$ which accomplishes the p_{in} requested for a fixed distribution of $\dot{m}_{WF}$ among the two port (k_1, k_2) can be predicted through Eq. (16). Obviously, the model provides a preliminary design which should be furtherly refined through a more complex numerical model which removes the assumption made on k_1, k_2, $\eta_{vol,glob}$, $\eta_{vol,main}$ and $\eta_{vol,dual\ int}$. Thus, equating the left-end side term of Eq. (16) with that of Eq. (12), it is possible to define $V_{dual\ int,end}$ (Eq. (20)) which allows that single SIP and DIP expander ensure the same intake pressure when $\dot{m}_{WF}$, Z, R, $T_{int,end}$, N_v and ω are the same. In Eq. (12) and in Eq. (16), the term Δp_{loss} was simplified. It was experimentally assessed that the pressure losses between the start and the end of the intake phase Δp_{loss} are comparable in single and dual-intake phase.

$$\frac{V_{dual\ int,end}}{V_{int,end}} = \frac{(\eta_{vol,main}k_1 + \eta_{vol,dual\ int}k_2)}{\eta_{vol}} = \frac{\eta_{vol,glob}}{\eta_{vol}} \tag{20}$$

Eq. (20) shows a criterion which ensures the same intake pressure for a SIP or DIP machine. According to it, the ratio between the intake end vane volume of DIP and SIP expander must be equal to that of their volumetric efficiencies $\eta_{vol,glob}$ and η_{vol}.

Considering, for example, the experimental comparison reported in Section 3 between the SIP and DIP expander with the same $\dot{m}_{WF}$, the latter has a lower intake pressure with respect to the single one because the two terms of Eq. (20) are not the same. In fact the left terms is equal to 2.8 ($V_{dual\ int,end}$ = 15.2 cm^3 and $V_{int,end}$ = 5.4 cm^3) while the right one is equal to 1.39 ($\eta_{vol,dual\ int}$ = 0.58 and η_{vol} = 0.42). Thus, to satisfy Eq. (20), $V_{dual\ int,end}$ should be equal to 7.5 cm^3 with a reduction up to 50% of the initial volume. So, the downsizing of the expander is the right answer. The downsizing additionally allows the reduction of weight, size and mechanical power lost by friction but it should provide a comparable mechanical power with the original SIP expander. In conclusion, the downsizing of the expander (with respect to an original design with only a single intake port) is the engineering answer if a dual port technology is adopted.

The downsizing of the expander can be performed reducing the height of the machine W_{exp} or the eccentricity *ecc*, which can be varied changing the stator diameter d_{stat} or the rotor diameter d_{rot}, respecting some geometrical constraints mainly related to the number of blades. Thus, the same design vane volume can be reached with several expander configurations. In order to find the best choice, a dedicated subroutine was added to the theoretical model in order to find the best choice related to the stator diameter and height (aspect ratio). The best choice means the minimization of the mechanical power lost by friction which still remains the weakest point. Indeed, Eqs. (5), (6.1), (6.2) and (6.3) allow to evaluate the effects of the expander geometry on the mechanical loss due to the dry friction at the blade tip: this choice is a good approximation of the total amount of mechanical power lost,

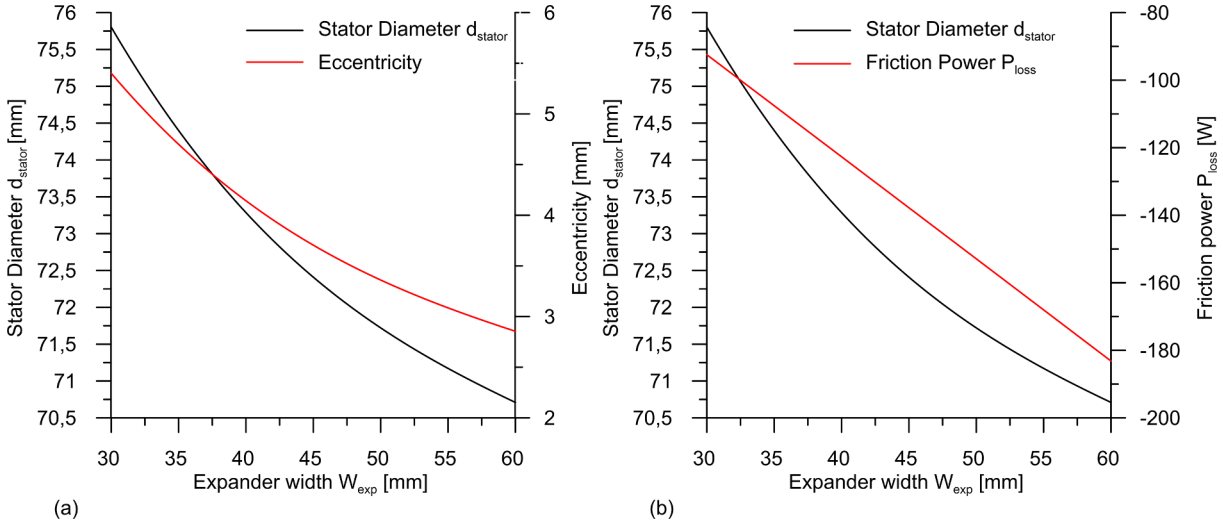

Fig. 9. (a) Boundaries on stator diameter, eccentricity and expander's width matching the same $V_{dual\ int,end}$ (7.5 cm^3) (b) resulting friction power P_{loss} according to the geometry of the machine.

being the other friction contributions negligible (motion of the blade inside the rotor's slot - side friction - and on the covers). Thus, the subroutine is based on the expression of the vane volume as a function of the two parameters considered to be optimized (eccentricity *ecc* and expander height W_{exp}), Eqs. (21.1) and (21.2).

$$V(\theta)_{vane} = \left(r_1 r_2 \frac{\sin\left(\frac{2\pi}{N_v}\right)}{2} - \frac{\pi r_{rotor}^2}{N_v} + r_{stator}^2 (\theta_c - \cos\theta_c \sin\theta_c) - \frac{Tk_b}{2}(r_1 + r_2 - 2r_{rotor}) \right) W_{exp} \tag{21.1}$$

$$\theta_c = \frac{\left(\theta_2 - \sin^{-1}\left(\frac{ecc\sin\theta_2}{r_{stator}}\right)\right) - \left(\theta_1 - \sin^{-1}\left(\frac{ecc\sin\theta_1}{r_{stator}}\right)\right)}{2} \tag{21.2}$$

where:

- θ_1 and θ_2 are the chamber start and end angle with respect to the eccentricity angle ($\theta = 0$) according to the convention reported in Fig. 2. They are given by Eqs. (21.3) and (21.4):

$$\theta_1 = \theta - \frac{2\pi}{2N_v} \tag{21.3}$$

$$\theta_2 = \theta - \frac{2\pi}{2N_v} \tag{21.4}$$

- r_1 (Eq. (21.5)) and r_2 (Eq. (21.6)) represents the distance from the center of the rotor to the start and the end of the chamber respectively.

$$r_1(\theta) = -ecc\cos\theta_1 + \sqrt{r_{stator}^2 + ecc^2(cos^2\,\theta_1 - 1)} \tag{21.5}$$

$$r_2(\theta) = -ecc\cos\theta_2 + \sqrt{r_{stator}^2 + ecc^2(cos^2\,\theta_2 - 1)} \tag{21.6}$$

For a specific $V_{dual\ int,end}$ (equal to 7.5 cm^3 for the specific case according to Eq. (20)), the solution of Eq. (20), varying the stator diameter d_{stator} and the expander width W_{exp}, produces the results shown in Fig. 9. In Fig. 9(a) the black curve represents d_{stator} values which ensure to achieve the specific $V_{dual\ int,end}$ varying W_{exp}. From d_{stator} vs expander width W_{exp}, the eccentricity (represented by the red curve) can be immediately derived being the rotor diameter kept equal to the original value (65 mm). Obviously, when W_{exp} decreases the d_{stator} must grow, being the volume constant. In Fig. 9(b) the effect on the friction power calculated by means of Eq. (5) was shown.

The results reported in Fig. 9(b) shows how the power lost by friction can be achieved with an expander with W_{exp} = 30 mm and d_{stator} = 75.9 mm. Indeed, in Fig. 9(b) the red curve representing friction power loss P_{loss} shows that the lowest value was ensured for W_{exp} equals to 30 mm. If W_{exp} is 30 mm to ensure the required $V_{dual\ int,end}$, the stator diameter must be equal to 75.9 mm as outlined by the black curve. Thus, the optimal expander configuration was identified: it must have the original d_{stator} and a W_{exp} reduced by a factor of two, with respect to the SIP expander. This means that at pre-design phase, a desired volume machine can be achieved reducing as much as possible W_{exp}. In a nutshell, the shape of the expander must be more oriented to a "disk" than to a "finger" in order to minimize the power lost by friction.

5.4. DDIP, DIP and SIP numerical comparison

As already observed, a more detailed modeling must be used in order go deep inside the results given by the simplified procedure. This will behave also as a verification procedure of the analytical simplified method. For this aim, the numerical GT-Suite™ model described in Section 5 was adopted to verify the conclusions of the analytical approach. The GT-Suite™ based model removes the assumptions introduced in the analytical model (represented by the Eqs. (9)–(19)) and allows to consider all the real phenomena related to the filling of two consecutive vanes (where the second filling happens after a previous one). The results reported in Fig. 10 have been obtained thanks to this comprehensive physically based model. The results – Fig. 10(a) - show that the simplified analytical model agrees with the fully comprehensive model. The lowest W_{exp} with the original d_{stator} ensures to achieve the minimum power lost due to friction. Moreover, for this design choice, the expander shows also the maximum indicated and mechanical power. In fact, in Fig. 10(b) the numerical prediction of the friction losses P_{loss} was compared with that provided by the analytical model. Despite it allows to reproduce the correct trend of the friction power as function of W_{exp} (and d_{stator}), it underestimates the mechanical power lost P_{loss}. In fact, there is an off-set between the analytical prediction (red upper curve) and the numerical one by GT-Suite™ procedure (magenta lower curve): this is due to the assumption on p_{rot} (the pressure of the working fluid enclosed in the gap between the blade bottom and the rotor slot), which was initially imposed equal to $p_{int}/2$

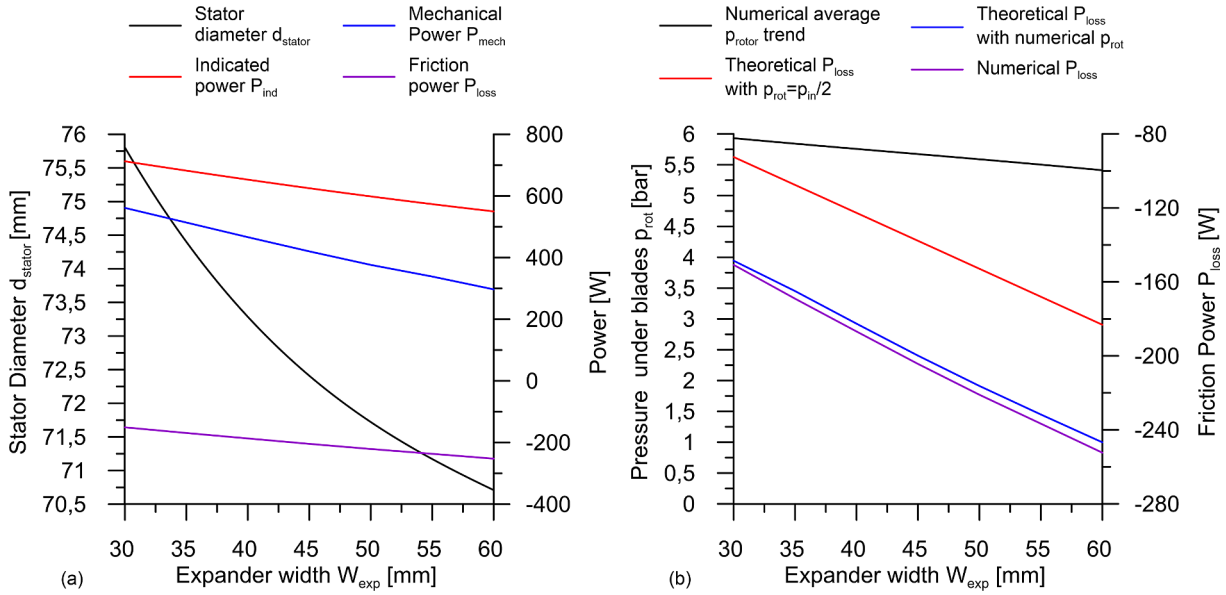

Fig. 10. Effects of d_{stator} and W_{exp} selection on P_{ind}, P_{mech}, P_{loss} (a); p_{rot} variation as function of W_{exp} and d_{stator} and comparison between theoretical and numerical model predictions.

in the theoretical model, for sake of simplicity. p_{rot} produces a contribution on the normal force which, together with the centrifugal force, participates to the normal force F_n which defines the power lost by friction through Eq. (4). Thus, the difference between the value of p_{rot} assumed equal to $p_{int}/2$ (4.38 bar) in the analytical model with the value predicted by the numerical model (linearly decreasing between 6 bar and 5.5 bar, when W_{exp} increases according to the GT-Suite™ platform) explains the underestimation provided by sub-routine. Hence, introducing the numerical predictions of p_{rot} in the theoretical analytical model, the friction power prediction, represented in Fig. 10(b) by the blue curve, fully coincides with the numerical results: this gives to the sub-routine friction analysis a wide validity. It can be safely used as a preliminary design of a dual-intake expander.

For the considered case, the previous analysis states that the best configuration has a W_{exp} = 30 mm and a d_{stator} = 75.9 mm. Thus, the downsized DIP has the same geometry (Table 2) of the SIP and DIP expanders (blade length and width, rotor and stator diameters, angular extent of intake and exhaust port) with the exception of W_{exp} which was decreased up to 50% of its original dimension (W_{exp} = 60 mm).

These data were introduced in the numerical GT-Suite™ based model and the performances of the DDIP were predicted and compared with the experimental ones of the SIP and DIP. To demonstrate the effectiveness of the DDIP solution, also the downsized SIP (DSIP) was considered and compared with the other machines. The DSIP is equal to DDIP with the only difference that in DSIP keeps a single intake port. In other words, DSIP is directly obtained from the SIP, downsizing it adopting a W_{exp} equal to 30 mm and keeping constant all the other dimensions. The comparison was carried out considering for SIP and DSIP the model developed and validated by the author in [33] and for DIP and DDIP the model developed in Section 4. The comparison was carried out considering that all the machines have the same clearance gap and friction coefficient defined in [33] and reported in Table 6. In particular, the friction coefficient C_{tip} was kept constant to 0.01 taking into account the oil hydrodynamic lubrication and the absence of permanent contact between the blades tip and the stator surface.

In Fig. 11 and in Table 6, the resulting indicated cycles and performances of the machines were compared: the original SIP and DIP (made by re-machining a second port on the original single-intake machine) are reported in Fig. 11(a) while the respective downsized version DDIP and DSIP in Fig. 11(b). From Fig. 11(a) it is evident how the SIP operates with a 50% higher intake pressure (10.7 bar) than the DIP one (5.50). The p_{in} increase ensures that the SIP P_{ind} (1432 W) is quite double than the DIP one (760 W) showing a strict relation between p_{in} and P_{ind}. Concerning P_{mech}, the difference between DIP and SIP it is similar to that of P_{ind} because the η_{mech} of DIP is slightly lower but comparable to the value of the SIP one (Table 6). Indeed, this happens because the P_{loss} of DIP (80 W) is lower than SIP one (90 W) but being the P_{ind} of SIP higher than that of DIP, the η_{mech} of SIP is slightly higher but comparable in accordance to the theoretical expectation (Eq. (7)). On the other hand, DIP machine shows higher η_{vol}, η_{ind} and η_{exp} than SIP due to the lower intake pressure. This means that, despite the DIP has a power deficit, it is more efficient than the SIP one from a thermo-fluid-dynamic point of view.

However, the downsizing of DIP (DDIP) allows to reduce this power deficit as confirmed by Fig. 11 and Table 6. Indeed, p_{in} in the case of DDIP is quite equal to that of the SIP one and consequently also P_{ind} is comparable as the one of DDIP (1276 W).

Moreover, in terms of P_{mech}, DDIP is comparable with SIP (P_{mech} of the DDIP is 8% lower than the SIP one) due the higher η_{mech} ensured by DDIP (Table 6). Indeed, the downsizing leads to a 50% lower P_{loss} and a lower impact on P_{ind} (Eq. (7)) and this provides that P_{ind} of DDIP decreases less than SIP for friction phenomena. Furthermore, η_{vol} improves with the DDIP adoption while η_{ind} and η_{exp} are comparable. On the other hand, these parameters are lower with respect to DIP. This means that the downsizing causes an increase of the power of the DIP at the expense of an efficiency reduction. The main reason of this efficiency reduction is due to the increase of the isochoric expansion with downsizing (Fig. 11(b)): in this case, in fact, a greater sudden expansion happens at exhaust port opening[1]. However, this effect can be easily mitigated redesigning the position of the exhaust port.

If the downsizing was performed directly on SIP (DSIP), the results show (Fig. 11(b) and Table 6) that keeping constant the $\dot{m}_{WF}$ entering the machine, p_{in} increases up to 50% with respect to the SIP and DDIP. This can be analytically demonstrated through Eq. (16): in the case of DSIP there is no contribution of k_2. So, keeping constant all the parameters, if $V_{int,end}$ diminishes with respect to SIP, p_{in} raises. Nevertheless, a higher p_{in} needs a greater intake temperature such that the fluid enters the machine at least in saturated vapor state. In order to ensure at DDIP inlet a superheating degree of 10 °C (retained to be the best operating condition at expander inlet) a T_{in} of 111.5 °C is needed while for SIP, DDIP and DIP T_{in} is respectively equal to 88.8 °C, 86.2 °C and 60.1 °C. This means that keeping constant $\dot{m}_{WF,}$ a higher thermal power must be recovered by the working fluid from the high thermal source. If this extra thermal power was not available, the working fluid entering the DDIP would not be completely vaporized and, in the worst cases, it could be in saturated state (liquid-vapor mixture) preventing the correct operation or even the machine startup. In any case, the operating conditions are far from the design ones. On the other hand, even if the thermal power recovered by the fluid is sufficient to ensure that the fluid enters the DSIP as superheated vapor, the machine works with a too high p_{in}. Therefore, the design machine must be updated in terms of thicknesses and sealing systems.

5.5. Downsizing effect on mechanical efficiency

As reported in Table 6, the downsizing leads to a higher mechanical efficiency η_{mech} with respect to the original machine. DDIP and DSIP has η_{lmech} equal to 97 % and 96 % respectively while the ones of SIP and DIP is 94 % and 90 %. This is in accordance with the theoretical expectation (Eqs. Eqs. (5), (6.1), (6.2) and (6.3)) according to which the mechanical power lost by friction P_{loss} should decrease reducing the expander dimension (DDIP and DSIP). Indeed, if the operating conditions do not vary, P_{loss} depends on the normal force F_n applied on the blades which depends exclusively on the expander geometry and the relative pressure under the blades (Eq. (6.3)).

So, it is theoretically expected that F_n is equal for SIP and DIP and diminishes for the downsized machine DDIP and DSIP. This aspect was demonstrated by the results of the numerical model shown in Fig. 12(a) where the F_n for SIP, DIP, DDIP and DSIP was reported as a function of $\dot{m}_{WF}$. As Fig. 12(a) shows when $\dot{m}_{WF}$ increases from 0.05 to 0.2 kg/s, F_n varies in ranges between 190–235 N for SIP, 180–200 N, for DIP,

Table 6
Comparison between SIP, DIP, DSIP and DDIP.

	SIP	DIP	DSIP	DDIP
Model parameter				
Clearance between vane tip and Stator [μm]	85	85	85	85
Clearance between blade tip and Stator [μm]	10	10	10	10
Clearance between rotor face and slot [mm] (equivalent orifice diameter)	0.2	0.2	0.2	0.2
Friction Coefficient at tip blade	0.01	0.01	0.01	0.01
Expander performance				
Intake pressure p_{in} (at intake manifold) [bar]	12.74	5.85	21.89	11.41
Intake end pressure p_{in} [bar]	10.70	5.50	20.26	11.07
Intake temperature [°C]	88.8	60.1	111.5	86.2
Elaborated mass flow rate m_{wf} [kg/s]	0.130	0.130	0.130	0.130
Mechanical power P_{mech} [W]	1342	680	1230	1817
Power loss P_{loss} [W]	90	80	46	60
Indicated Power P_{ind} [W]	1432	760	1276	1877
Global efficiency η_{glob} [%]	47	55	47	46
Mechanical Efficiency [%]	94	90	97	96
Volumetric Efficiency [%]	51	72	56	75
Indicated Efficiency ± 2.5% [%]	50	61	49	48

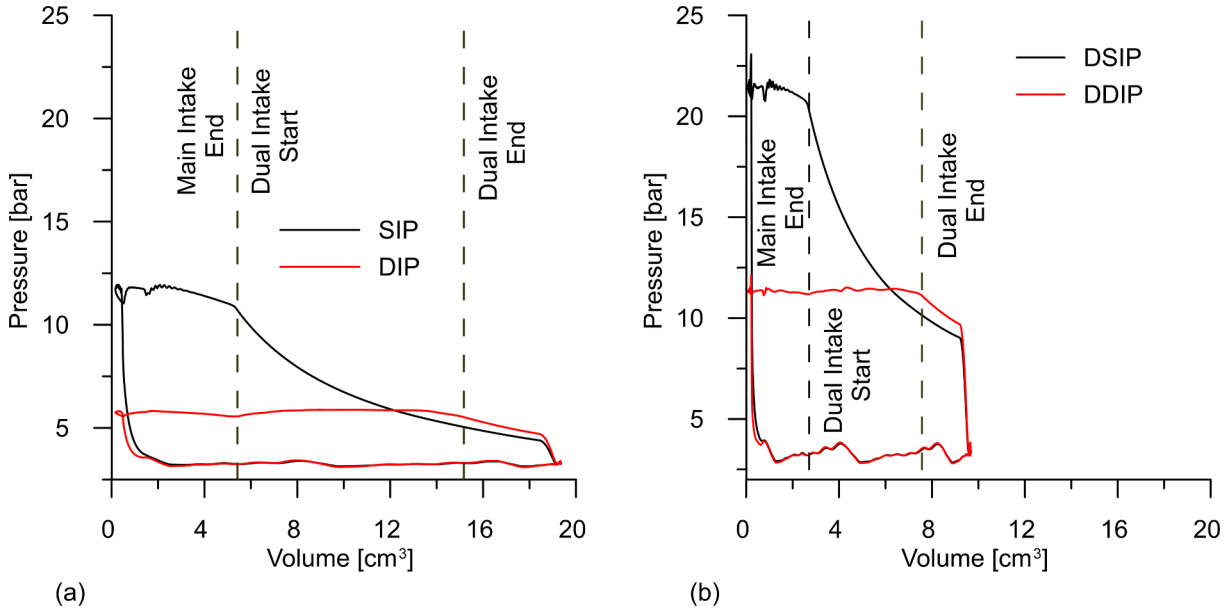

Fig. 11. Indicated cycle of SIP and DSIP expander (a); Indicated cycle of DIP and DDIP expander (b).

97–130 N for DDIP and 115–205 N for DSIP expander. Thus, F_n of SIP and DIP is comparable while decreases with the downsizing of the machine (DDIP and DSIP) except for DSIP when $\dot{m}_{WF}$ tends to 0.2 kg/s. Being F_n given by the sum of centrifugal F_c and pressure F_p force, the analysis of this two contributes was numerically carried out to understand the F_n difference between the machines. In Fig. 12(b) F_c of the four machines was reported. It is clear from Fig. 12(b) that F_c depends only by the machine geometry as it does not depend on $\dot{m}_{WF}$. In fact, F_n is equal for SIP and DIP (21.9 N) and decreases with machine downsizing in DDIP and DSIP (11 N).

Concerning F_p, in Fig. 12(c) it is evident its dependence on $\dot{m}_{WF}$. In particular F_p grows with $\dot{m}_{WF}$ for SIP (170–213 N), DIP (160–180 N) and for the DDIP (86–120 N) and DSIP (100–194 N) because $\dot{m}_{WF}$ raise causes the growth of pressure of the fluid enclosed under blade p_{rot} (while $p_{ext,env}$ remains constant) as it can be seen in Fig. 12(d). F_p is lower in the DDIP and DSIP nonetheless Fig. 12(d) shows that p_{rot} in these machines is higher than SIP and DIP. In fact, in DDIP and DSIP the fluid under the blades is enclosed in a lower volume (2,5 cm^3) with respect to the machines with the original geometry (5 cm^3). However, this aspect has a lower impact on F_p than geometry reduction (on which F_p depends for Eq. (6.2)). Indeed, although p_{rot} raises with downsizing, the surface of the blade bottom on which the fluid pressure acts diminishes in a greater way leading to a reduction of F_p in DDIP and DSIP (Fig. 12(c)) machine. Moreover, it is worth noting how F_p is higher than F_c for each machine representing the 85–90% of the whole F_n. Thus, the fluid enclosed under the blade has a greater role on P_{loss} with respect to the centrifugal force Fc applied on the blade. This knowledge gives the design direction to increase as much as possible the rotor slots to reduce F_p. Therefore, the results reported in Fig. 12 shows that the advantages offered by the downsizing (and in general by the dual intake technology) should be even higher than that reported in Table 6.

In conclusion, the use of dual-intake port in SVRE design is suggested. It can be adopted to perform a downsizing of the original machine with a similar P_{mech}. In fact, despite the DIP has a greater efficiency than SIP, since it works with a 50% lower intake pressure it does not ensure to produce the same P_{mech}. Therefore, the downsizing allows to fill this power gap and to introduce benefits on expander weight, dimension and mechanical efficiency. In this case, the same inlet pressure can be kept constant as in the case of SIP. Otherwise, the dual-intake port can be easily done on a pre-existing single-intake expander and to keep the same intake pressure more mass flow rate must be aspirated by the machine as done in [32]. This allows to manage higher working fluid mass flow rates with respect to the design value, allowing a stronger recovery if this could be possible (avoiding, for instance, a partial bypass of the exhaust gases in the case of excess of heat to be recovered with respect to the design value or in presence of other hot sources which could be considered).

6. Conclusions

In this paper, the benefits provided by the adoption of the dual-intake port technology in the SVRE design was analyzed. This represents an additional and novel contribution in the direction of designing the component, having already observed the advantages obtained simply opening another intake port in an existing machine. In fact, the dual-intake port was never conceived as a design alternative of a traditional SVRE.

The simple introduction of an additional intake port to an existing SVRE expander causes, if the inlet pressure of the machine is kept constant, an increase of the permeability of the machine and, therefore, a working fluid mass flow rate increase: the expander is simply able to induct a greater mass flow rate without any other intervention. This could be interesting if an excess of heat is available with respect to the designed value or in the case of the integration of other high temperature thermal sources. This feature could appear particularly useful in order to increase the flexibility of the machine and operate at strong off design conditions considering that a second port can be easily opened or closed.

For a specific design condition (for a desired mass flow rate), the adoption of the dual-intake option allows to reduce the inlet pressure of the expander and this appears an interesting feature allowing the ORC-based recovery unit to operate with a lower maximum pressure at the expense of a lower mechanical power. This was observed trough an experimental comparison between single and dual-intake expander with the same geometry and mass flow rate. The two machines were installed on an ORC-based power unit built to recover the energy of the exhaust gases of a 3 L supercharged diesel engine. This comparison was fundamental to understand the filling behavior of the two machines and to define the main physical parameters useful in the design phase. Further experimental evidences were the followings:

- the dual-intake expander DIP shows a lower intake pressure because

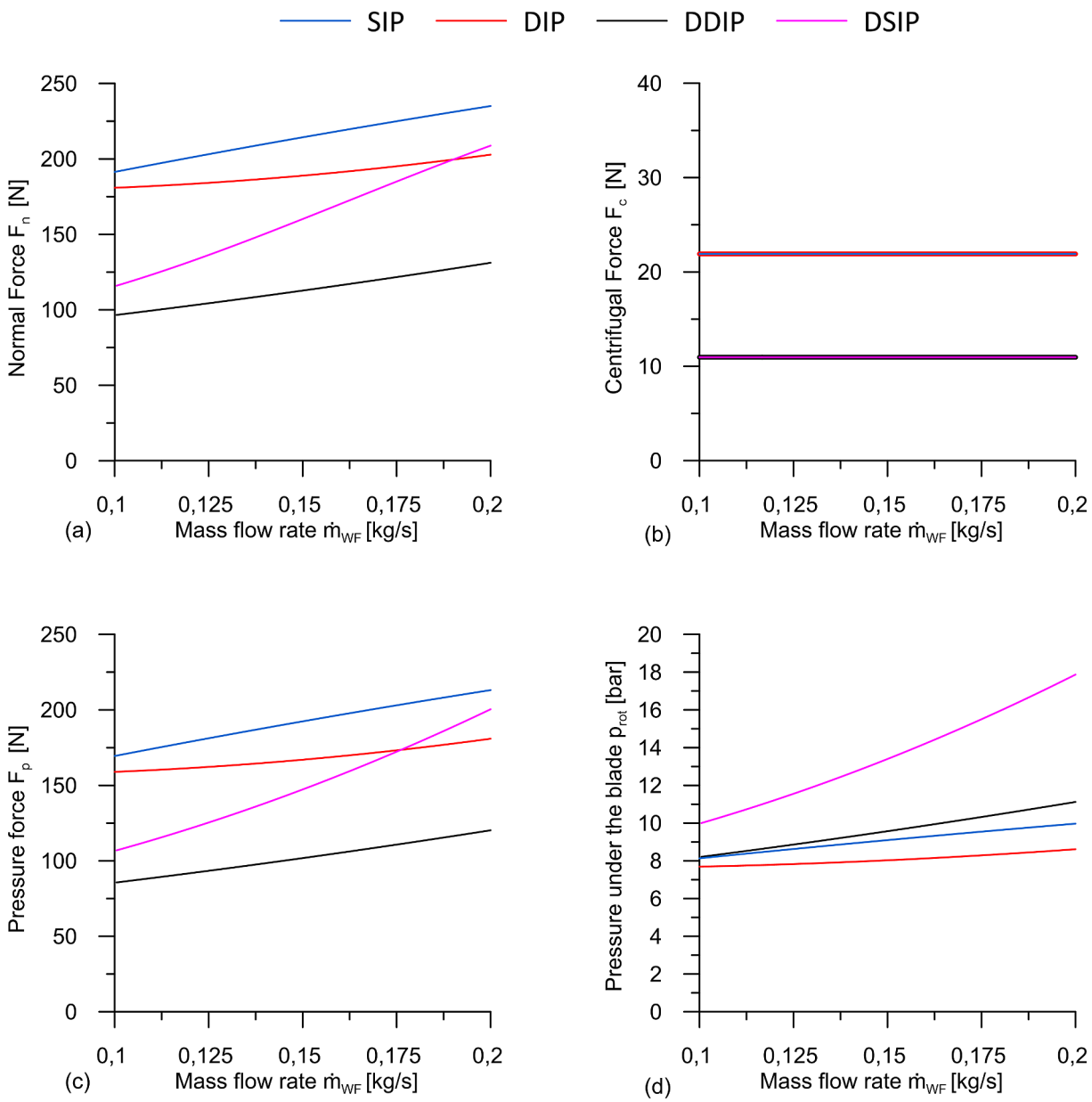

Fig. 12. Normal Force F_n (a), Centrifugal Force F_c (b), Pressure Force (c) and pressure of fluid under the blades p_{rot} (d) for SIP, DIP, DDIP and DSIP varying $\dot{m}_{WF}$.

the mass flow rate does not exclusively enter the machine through the main port but also through the additional one;

- if the adduction pipes to the ports have the same cross section, the mass flow rate tends to flow inside the machine mostly through the second intake port, due to the higher vane volume during filling, even though the vane is already partially filled via the first port.
- Despite the DIP produces a partial recovery due to the indicated cycle modifications, the mechanical power is lower than the single intake port case for a fixed mass flow rate.

Therefore, in order to set up preliminarily the design of the expander with a dual-port option which ensures the same inlet pressure and produced mechanical power of a single port machine (SIP) for the same design working fluid flow rate, an analytical model was developed. The model solves in a closed form the problem showing that a significant downsizing of the machine is possible. Considering that the downsizing of the machine can be reached following different geometry choices, the model indicates the optimum shaping of the expander, which minimizes the power lost by friction, favoring a “disk” shaped expander rather than a “finger” type one. The optimum geometry given by the analytical model was verified by means of a more complex and comprehensive model developed in GT-Suite™ which represents:

(a) a transient filling and emptying of the vanes via a 1-D approach;
(b) a lumped parameter model during vane rotation for the thermodynamic properties;
(c) a quasi-steady leakage flow across blades at tip, at the bottom and side of the slots on the rotor and at the lateral “closing” planes of the machine;
(d) a dynamic model concerning blade motion inside the slots and during rotation;
(e) a detailed calculation of the indicated power and friction power.

It was furtherly observed that:

- in the downsized double port machine DDIP, the volume reduction was of the order of 50% of the original single port machine, keeping constant the same machine inlet pressure and working fluid flow

rate. The downsized expander produces a comparable mechanical power (with respect to the original single-port machine at the same working fluid flow rate) allowing to fill the power gap encountered with the original DIP. This is a very interesting result because a smaller machine has lower friction losses (-50%). The weight of the machine decreases too, with evident additional benefits (encumbrance improvement) particularly interesting for on-board applications;

- The downsizing should be performed only with the introduction of a dual intake port configuration. Indeed, the downsized SIP (DSIP) works with a 50% higher intake pressure than SIP and DSIP when the mass flow rate entering the machine is the same. Thus, it requires a higher thermal power to work in proper condition and if this is not enough the fluid enters the machine as liquid or liquid vapor mixture preventing the startup and correct operating conditions of the machine. Moreover, even though the thermal power is sufficient, the high-pressure value lead to a components size and cost increase.

CRediT authorship contribution statement

Fabio Fatigati: Conceptualization, Investigation, Software, Data curation, Validation, Formal analysis, Methodology, Supervision, Writing - original draft, Writing - review & editing. **Marco Di Bartolomeo:** Data curation, Validation, Writing - original draft, Writing - review & editing. **Davide Di Battista:** Data curation, Validation, Writing - original draft, Writing - review & editing. **Roberto Cipollone:** Formal analysis, Methodology, Supervision, Writing - original draft, Writing - review & editing.

Declaration of Competing Interest

The authors declare that they have no known competing financial interests or personal relationships that could have appeared to influence the work reported in this paper.

Acknowledgments

The authors would like to acknowledge Ing. Enea Mattei S.p.A, its CEO, Dr. Giulio Contaldi and Dr. Stefano Murgia for the support given during this research activity.

References

[1] Pili Roberto, Romagnoli Alessandro, Kamossa Kai, Schuster Andreas, Spliethoff Hartmut, Wieland Christoph. Organic Rankine Cycles (ORC) for mobile applications – economic feasibility in different transportation sectors. Appl Energy 2017;204:1188–97. https://doi.org/10.1016/j.apenergy.2017.04.056.

[2] Zhao Meng, Wei Mingshan, Song Panpan, Liu Zhen, Tian Guohong. Performance evaluation of a diesel engine integrated with ORC system. Appl Therm Eng 2017;115:221–8. https://doi.org/10.1016/j.applthermaleng.2016.12.065. ISSN 1359-4311.

[3] Galindo J, Ruiz S, Dolz V, Royo-Pascual L, Haller R, Nicolas B, et al. Experimental and thermodynamic analysis of a bottoming Organic Rankine Cycle (ORC) of gasoline engine using swash-plate expander. Energy Convers Manage 2015;103:519–32. https://doi.org/10.1016/j.enconman.2015.06.085.

[4] Shu Gequn, Zhao Mingru, Tian Hua, Huo Yongzhan, Zhu Weijie. Experimental comparison of R123 and R245fa as working fluids for waste heat recovery from heavy-duty diesel engine. Energy 2016;115(Part 1):756–69. https://doi.org/10.1016/j.energy.2016.09.082.

[5] Zhang Ye-Qiang, Yu-Ting Wu, Xia Guo-Dong, Ma Chong-Fang, Ji Wei-Ning, Liu Shan-Wei, et al. Development and experimental study on organic Rankine cycle system with single-screw expander for waste heat recovery from exhaust of diesel engine. Energy 2014;77:499–508. https://doi.org/10.1016/j.energy.2014.09.034.

[6] Di Battista Davide, Di Bartolomeo Marco, Villante Carlo, Cipollone Roberto. On the limiting factors of the waste heat recovery via ORC-based power units for on-the-road transportation sector. Energy Convers Manage 2018;155:68–77. https://doi.org/10.1016/j.enconman.2017.10.091. ISSN 0196-8904.

[7] Mavrou Paschalia, Papadopoulos Athanasios I, Seferlis Panos, Linke Patrick. Spyros Voutetakis, Selection of working fluid mixtures for flexible Organic Rankine Cycles under operating variability through a systematic nonlinear sensitivity analysis approach. Appl Therm Eng 2015;89:1054–67. https://doi.org/10.1016/j.applthermaleng.2015.06.017.

[8] Rahbar Kiyarash, Mahmoud Saad, Al-Dadah Raya K, Moazami Nima, Mirhadizadeh Seyed A. Review of organic Rankine cycle for small-scale applications. Energy Convers Manage 2017;134:135–55. https://doi.org/10.1016/j.enconman.2016.12.023. ISSN 0196-8904.

[9] Yan Jiayao, Han Yongqiang, Tian Jing, Yun Xu, Zhang Yiming, Chen Ruolong. Performance investigation of a novel expander coupling organic Rankine cycle: Variable expansion ratio rotary vane expander for variable working conditions. Appl Therm Eng 2019;152:573–81. https://doi.org/10.1016/j.applthermaleng.2019.02.103. ISSN 1359-4311.

[10] Qiu Guoquan, Liu Hao, Riffat Saffa. Expanders for micro-CHP systems with organic Rankine cycle. Appl Therm Eng 2011;31(16):3301–7. https://doi.org/10.1016/j.applthermaleng.2011.06.008. ISSN 1359-4311.

[11] Pantano Fabio, Capata Roberto. Expander selection for an on board ORC energy recovery system. Energy 2017;141:1084–96. https://doi.org/10.1016/j.energy.2017.09.142. ISSN 0360-5442.

[12] Quoilin S. Sustainable Energy Conversion through the use of Organic Rankine Cycles for Waste Heat Recovery and Solar Applications PhD thesis Belgium: University of Liège; 2011

[13] Dumont Olivier, Parthoens Antoine, Dickes Rémi, Lemort Vincent. Experimental investigation and optimal performance assessment of four volumetric expanders (scroll, screw, piston and roots) tested in a small-scale organic Rankine cycle system. Energy 2018;165(Part A):1119–27. https://doi.org/10.1016/j.energy.2018.06.182. ISSN 0360-5442.

[14] Bao Junjiang, Zhao Li. A review of working fluid and expander selections for organic Rankine cycle. Renew Sustain Energy Rev 2013;24:325–42. https://doi.org/10.1016/j.rser.2013.03.040. ISSN 1364-0321.

[15] Pardeep Garg GM, Karthik Prashant Kumar. Pramod Kumar, Development of a generic tool to design scroll expanders for ORC applications. Appl Therm Eng 2016;109(Part B):878–88. https://doi.org/10.1016/j.applthermaleng.2016.06.047.

[16] Song Panpan, Wei Mingshan, Zhang Yangjun, Sun Liwei, Emhardt Simon, Zhuge Weilin. The impact of a bilateral symmetric discharge structure on the performance of a scroll expander for ORC power generation system. Energy 2018;158:458–70. https://doi.org/10.1016/j.energy.2018.06.053. ISSN 0360-5442.

[17] Papes Iva, Degroote Joris, Vierendeels Jan. New insights in twin screw expander performance for small scale ORC systems from 3D CFD analysis. Appl Therm Eng 2015;91:535–46. https://doi.org/10.1016/j.applthermaleng.2015.08.034. ISSN 1359-4311.

[18] Stošić N, Smith IK, Kovačević A, Aldis CA. The design of a twin-screw compressor based on a new rotor profile. J Eng Des 1997;8(4):389–99. https://doi.org/10.1080/09544829708907973.

[19] Imran Muhammad, Usman Muhammad, Park Byung-Sik, Lee Dong-Hyun. Volumetric expanders for low grade heat and waste heat recovery applications. Renew Sustain Energy Rev 2016;57:1090–109. https://doi.org/10.1016/j.rser.2015.12.139. ISSN 1364-0321.

[20] Smith IK, Stosic N, Kovacevic A. Screw expanders increase output and decrease the cost of geothermal binary power plant systems. Trans- Geotherm Resour Counc 2005;29:787–94.

[21] Smith IK, Stosic N, Kovacevic A. Power recovery from low cost two-phase expanders. In: Proceedings of the GRC annual meeting: San Diego, California; 2001.

[22] Eyerer Sebastian, Dawo Fabian, Rieger Florian, Schuster Andreas, Aumann Richard, Wieland Christoph, Spliethoff Hartmut. Experimental and numerical investigation of direct liquid injection into an ORC twin-screw expander. Energy 2019;178:867–78. https://doi.org/10.1016/j.energy.2019.04.172. ISSN 0360-5442.

[23] Clemente Stefano, Micheli Diego, Reini Mauro, Taccani Rodolfo. Bottoming organic Rankine cycle for a small scale gas turbine: a comparison of different solutions. Appl Energy 2013;106:355–64. https://doi.org/10.1016/j.apenergy.2013.02.004. ISSN 0306-2619.

[24] Chiong MC, Rajoo S, Romagnoli A. Nozzle steam piston expander for engine exhaust energy recovery. SAE technical paper 2015-01-0126.

[25] Han Yongqiang, Li Runzhao, Liu Zhongchang, Tian Jing, Wang Xianfeng, Kang Jianjian. Feasibility analysis and performance characteristics investigation of spatial recuperative expander based on organic Rankine cycle for waste heat recovery. Energy Convers Manage 2016;121:335–48. https://doi.org/10.1016/j.enconman.2016.05.042. ISSN 0196-8904.

[26] Musthafah MT, Yamada N. Thermodynamic analysis of expansion profile for displacement-type expander in low-temperature Rankine cycle. J Therm Sci Technol 2010.

[27] Badr O, O'Callaghan PW, Hussein M, Probert SD. Multi-vane expanders as prime movers for low-grade energy organic Rankine-cycle engines. Appl Energy 1984;16(2):129–46. https://doi.org/10.1016/0306-2619(84)90060-6. ISSN 0306-2619.

[28] Mohd M, Tahir NY, Hoshino T. Efficiency of compact organic Rankine cycle system with rotary-vane-type expander for low-temperature waste heat recovery. Int J Environ Sci Eng 2010;2(1):11–6.

[29] Yang B, Peng X, He Z, Guo B, Xing Z. Experimental investigation on the internal working process of a CO2 rotary vane expander. Appl Therm Eng 2009;29(11–12):2289–96. https://doi.org/10.1016/j.applthermaleng.2008.11.023.

[30] Vodicka Vaclav, Novotny Vaclav, Zeleny Zbynek, Mascuch Jakub, Kolovratnik Michal. Theoretical and experimental investigations on the radial and axial leakages within a rotary vane expander. Energy 2019;189. https://doi.org/10.1016/j.energy.2019.116097. ISSN 0360-5442.
[31] Collings P, Yu Z. Numerical analysis of an organic rankine cycle with adjustable working fluid composition, a volumetric expander and a recuperator. Energies 2017;10:440.
[32] Fatigati Fabio, Di Bartolomeo Marco, Cipollone Roberto. Dual intake rotary vane expander technology: experimental and theoretical assessment. Energy Conversand Manage 2019;186:156–67. https://doi.org/10.1016/j.enconman.2019.02.026. ISSN 0196-8904.
[33] Fabio Fatigati, Marco Di Bartolomeo, Davide Di Battista, Roberto Cipollone, Experimental and Numerical Characterization of the Sliding Rotary Vane Expander Intake Pressure in Order to Develop a Novel Control-Diagnostic Procedure, Energies, 12, 2019, 10, 1970, 1996-1073, DOI: 10.3390/en12101970.
[34] GT Suite, Flow Theory Manual, flow solver basics.

Io sottoscritto Fabio Fatigati, co-autore dell'articolo scientifico: "A dual-intake-port technology as a design option for a Sliding Vane Rotary Expander of small-scale ORC-based power units" pubblicato sulla rivista internazionale Energy Conversion and Management, (https://doi.org/10.1016/j.enconman.2020.112646), dichiaro che i contributi degli autori nello sviluppo del presente articolo sono i seguenti:

- **Fabio Fatigati**: Conceptualization, Investigation, Software, Data curation, Validation, Formal analysis, Methodology, Supervision, Writing - original draft, Writing - review & editing;
- Marco Di Bartolomeo: Data curation, Validation, Writing - original draft, Writing - review & editing;
- Davide Di Battista: Data curation, Validation, Writing - original draft, Writing - review & editing;
- Roberto Cipollone: Formal analysis, Methodology, Supervision, Writing - original draft, Writing - review & editing.

L'indicazione sui contributi degli autori è riportata nel *CRediT authorship contribution statement* a pagina 17 del medesimo articolo.

In fede, L'Aquila 24/09/2021

Fabio Fatigati